TAMPEREEN TEKNILLINEN YLIOPISTO
TAMPERE UNIVERSITY OF TECHNOLOGY

Tommi Hakulinen

Towards Stabilized, Short Pulse Q-switched Fiber Lasers

Julkaisu 905 • Publication 905

Tampere 2010

Tampereen teknillinen yliopisto. Julkaisu 905
Tampere University of Technology. Publication 905

Tommi Hakulinen

Towards Stabilized, Short Pulse Q-switched Fiber Lasers

Thesis for the degree of Doctor of Science in Technology to be presented with due permission for public examination and criticism in Tietotalo Building, Auditorium TB104, at Tampere University of Technology, on the 10th of September 2010, at 12 noon.

Tampereen teknillinen yliopisto - Tampere University of Technology
Tampere 2010

ISBN 978-952-15-2407-3 (printed)
ISBN 978-952-15-2608-4 (PDF)
ISSN 1459-2045

Abstract

This thesis concerns stable repetition rate, Q-switched fiber lasers using semiconductor saturable absorber mirrors (SESAMs) as elements triggering pulse operation. The nonlinear reflectivity responses of the SESAMs have been extensively studied to optimize their performance for different temporal regimes. The results reveal that the effective saturation fluence depends strongly on the pulse width providing that the saturation fluence for Q-switched operation is set individually since it differs significantly from the value observed for other regimes, e.g. for mode-locking. A simple method for determining the absorption recovery time of a SESAM has been proposed, based on the measurements of the nonlinear response using a source with variable pulse width.

The recovery time of the SESAM was controlled by Ni-ion irradiation followed by appropriate thermal annealing. The combination of these processes allows an optimal balance between fast and slow components in absorption recovery to be achieved. Furthermore, thermal annealing reduces the undesirable nonsaturable loss caused by ion irradiation, and improves the SESAM's long-term stability by removing short-lived defects.

A resonant SESAM with high modulation depth was used to achieve pulse width reduction. Such a saturable absorber mirror used in a short laser cavity resulted in demonstration of 8 ns pulses, which are the shortest pulses reported for passively Q-switched fiber lasers. The timing jitter of passively Q-switched fiber lasers is typically high and could reach tens of microseconds. An optically driven surface-normal modulator was used to ensure both passive Q-switching and stabilization of the pulse train, and resulted in substantial reduction of the timing jitter by a factor of 1.66×10^{3}.

To summarize the main aims of this thesis, this study is focused on the efficient approaches towards a simple, fiber based pulse source emitting short, energetic pulses forming a stable pulse train. Such a pulse source lends itself to various applications in material processing, medical instruments and scientific research.

Acknowledgments

The work presented in this thesis has been carried out in Optoelectronics Research Centre (ORC) of Tampere University of Technology during 2006–2008 under supervision of Prof. Oleg Okhotnikov. Without his enthusiasm and determination this thesis would never been finished, of which I owe the deepest gratitude. I also want to thank Prof. Emeritus Markus Pessa, the former director of ORC for giving me the opportunity to work in such a high-class international scientific atmosphere. I want to thank also the current director of ORC, Dr. Pekka Savolainen for supporting the finalizing stage of my thesis work.

My work has been financially supported by several parties: National Graduate School in Material Physics, Emil Aaltonen Foundation, Vilho, Yrjö and Kalle Väisälä Foundation, Finnish Foundation for Technology Promotion, and Jenny and Antti Wihuri Foundation. The author gratefully acknowledges this support.

This thesis presents the fruits of teamwork. I have had an honor to work with superb colleagues: I want to thank Prof. Mircea Guina for growing some of the semiconductor structures used in thesis and constant encouragement in my career. Dr. Robert Herda taught me the art of building mode-locked fiber lasers and formulated theoretical insight to support my articles. I owe a big Thank You to Dr. Matei Rusu, with whom I had the opportunity to work at ORC and Modulight. Matei's tremendous skills in various branches of engineering combined with a great sense of humor make him the best colleague that one can ask for. Dr. Samuli Kivistö was my closest colleague during my ORC years 2004–2008, with whom I shared the office and the joys and sorrows of everyday research work. Dr. Lasse Orsila deserves thanks for guiding me to the world of optical thin films. Special thanks for the design and evaporation of the etalon and dichroic structures used in paper 3. I want to thank the former and present members of Ultrafast and Intense Optics group, especially Dr. Antti Isomäki, Dr. Antti Härkönen, Esa Saarinen, Juho Kerttula, Jussi Rautiainen for valuable discussions and keeping up the good spirit.

This work could not have been done without the dedicated work of the MBE growers, in particular Dr. Soile Suomalainen, Riku Koskinen and Jari Lyytikäinen who have fabricated the SESAM structures used in this work. The help from Tero Kontkanen with electronics should not be forgotten. The kind help of Anne Viherkoski in administrative issues has made concentrating on scientific work possible. The whole staff of ORC has made this time enjoyable.

I want to thank Dr. Charis Reith for improving the linguistic impression of my articles and this thesis. The pre-examiners of this thesis, Prof. Seppo Honkanen and Dr. Scott Buchter helped me to improve the style of this thesis.

I have been privileged to enjoy the company of great friends. With some I have studied, with some sung in Teekkarikuoro, with others making interactive music theatre in NääsPeksi, and with some I have played in bands. Or just have had tons of fun. I want to thank you all for giving the valuable counterbalance to the work and studies.

In addition, I want to acknowledge the long-term support from my parents and other relatives.

The most sincere thanks go to my beloved wife Tuulia and our wonderful sons Aaro and Ilmari. You have made this life worth of living. Thank you!

Tampere, July 2010
Tommi Hakulinen

Table of Contents

List of Publications

The following papers are included in this dissertation as appendices. In the text, these publications are referred to as (P1)... (P4).

(P1) T. Hakulinen, R. Herda, and O. G. Okhotnikov, "Nonlinear Response of Saturable Absorber Mirrors for Different Operation Regimes," *IEEE Photonics Technology Letters,* Vol. 19, No. 5, pp. 333–335 (2007).

(P2) T. Hakulinen, R. Herda, and O. G. Okhotnikov, "Effect of post-epitaxial-growth processing on the nonlinear response of saturable absorber," *Applied Optics*, Vol. 47, No. 9, pp. 1235–1238 (2008).

(P3) T. Hakulinen and O. G. Okhotnikov, "8 ns fiber laser Q switched by the resonant saturable absorber mirror," *Optics Letters*, Vol. 32, No. 18, pp. 2677–2679 (2007).

(P4) T. Hakulinen, R. Koskinen, and O. G. Okhotnikov, "Low jitter Q-switched fiber laser using optically driven surface-normal saturable absorber modulator," *Optics Express*, Vol. 16, No. 12, pp. 8720–8726, (2008).

Related Publications

The following papers are related to this thesis but are not appended:

(RP1) S. Kivistö, T. Hakulinen, M. Guina, and O. G. Okhotnikov: Tunable Raman Soliton Source Using Mode-Locked Tm-Ho Fiber Laser, IEEE Photon. Techn. Lett., Vol. 19, No. 12, pp. 934–936 (2007)

(RP2) S. Kivistö, T. Hakulinen, A. Kaskela, B. Aitchison, D. P. Brown, A. G. Nasibulin, E. I. Kauppinen, A. Härkönen, and O. G. Okhotnikov, "Carbon nanotube films for ultrafast broadband technology," *Optics Express*, Vol. 17, No. 4, pp. 2358–2363 (2009).

(RP3) R. Herda, T. Hakulinen, S. Suomalainen, and O. G. Okhotnikov, "Cavity-enhanced saturable and two-photon absorption in semiconductors," *Applied Physics Letters*, Vol. 87, pp. 21111051–21111053, (2005).

(RP4) E. J. Saarinen, A. Härkönen, R. Herda, S. Suomalainen, L. Orsila, T. Hakulinen, M. Guina, and O. G. Okhotnikov: Harmonically Mode-Locked VECSELs for multi-GHz Pulse Train Generation, Optics Express, Vol. 15, Issue 3, pp. 955–964 (2007)

(RP5) L. Orsila, R. Herda, T. Hakulinen, and O. G. Okhotnikov: Thin-film Fabry-Pérot dispersion compensator for mode-locked fiber lasers, IEEE Photon. Techn. Lett, Vol. 19, No. 1, pp. 6–8 (2007)

Author's Contribution

This thesis is based on four original journal articles published in international peer-reviewed press and provided as appendices to the thesis. For all work reported, the author has designed and built the experimental test setups and performed the most of the investigative work. The author has also played a key role in reporting the results as well as writing the article manuscripts. However, the work presented in this thesis is a result of teamwork. The author has benefited from the contribution of the author's co-workers, especially in semiconductor crystal growing, designing and manufacturing of optical components as wells as theoretical modeling.

List of Abbreviations and Symbols

AOM	Acousto-Optic Modulator
AR	Anti-Reflection
ASE	Amplified Spontaneous Emission
BBO	Beta Barium Borate, β-BaB_2O_4
CNT	Carbon NanoTubes
cw	continuous wave
DBR	Distributed Bragg Reflector
DFB	Distributed FeedBack
EOM	Electro-Optic Modulator
FBG	Fiber Bragg Grating
FWHM	Full Width at Half Maximum
MBE	Molecular Beam Epitaxy
ML	Mode-Locking
MOFA	Master Oscillator Fiber Amplifier
MOPA	Master Oscillator Power Amplifier
LED	Light Emitting Diode
LD	Laser Diode
PECVD	Plasma Enhanced Chemical Vapor Deposition
QD	Quantum Dot
QS	Q-Switching
QSML	Q-Switched Mode-Locking
QW	Quantum Well
RTA	Rapid Thermal Annealing

SARM	Saturable Absorber Reflection Modulator
SESAM	SEmiconductor Saturable Absorber Mirror
TPA	Two-Photon Absorption
YAG	Yttrium Aluminum Garnet

α_{ns}	Nonsaturable loss
ΔR	Modulation depth
$\Delta\Omega_{lock}$	Locking bandwidth
E_p	Pulse energy
f_{rep}	Repetition rate
F_{sat}	Saturation fluence
λ	Wavelength
n	Refractive index
q_0	Nonsaturated loss coefficient
τ_p	Pulse width
τ_{rec}	Recovery time of absorption
t_{rt}	Cavity round-trip time

1. Introduction

"The light and heat of the sun; these are composed of minute atoms which, when they are shoved off, lose no time in shooting right across the interspace of air in the direction imparted by the shove." – Lucretius 55 BC *On the nature of the Universe.*

Light as a phenomenon has attracted mankind from the very early days. Fire in the form of light has provided comfort, safety and a means of signaling. Even the modern theory of wave-particle duality is already 100 years old (1). One particular emission source of light has been an active branch of study of physics in recent decades. Lasers (*Light Amplification by Stimulated Emission of Radiation)* have found their place in numerous applications in e.g. science, industry, medicine, and consumer electronics. Photonics as a branch of industry including lasers and fiber technology has developed since the 1980s, employing tens of thousands of people all over the world.

1.1 A brief history of laser development

Theoretical foundations of the laser were presented by Einstein in 1917 (2). The coefficients for absorption, spontaneous emission, and stimulated emission of electromagnetic radiation were derived. These coefficients are nowadays entitled Einstein coefficients, and present the probability of each process. The very first laser was built at the Hughes Aircraft Company by T.H. Maiman in May 15, 1960 (3), (4). The gain medium was a 2 cm long ruby (chromium in corundum) cylinder with 1 cm diameter. The ends were ground and polished flat and parallel and coated with silver. The laser was optically pumped by a spring-shaped xenon flashlight that surrounded the ruby cylinder. The output of the laser, at a wavelength of 694.3 nm, was taken through a 1 mm opening in the silver coating at one end of the cylinder. The first diode laser was developed by R. N. Hall *et al.* in 1962 at General Electric (5). It was a gallium-arsenide *p-n* junction emitting at the wavelength of 842 nm. The development of powerful and efficient diode lasers has been essential for fiber laser development due to their use as pump sources.

1.1.1 Fiber lasers

Lasers are commonly divided in different categories according to their gain media, which appear in all three forms of matter: gas, liquid, and solid. Gas lasers are typically pumped by electric discharges. Different gas lasers include e.g. CO_2 lasers, He-Ne lasers, and several excimer (e.g. KrF, ArF) lasers. Dye lasers usually have their gain medium in the form of liquid solution, e.g. rhodamine 6G. The common property of dye lasers is a broad gain bandwidth, which allows for wavelength tunability and/or short pulse generation. Solid-state lasers in principal cover all remaining lasers, but in practice e.g. semiconductor lasers, despite being solid, are considered a separate group from solid-state lasers. In solid-state lasers the gain

medium consists of the host and dopant. The host media include glass, crystal, and fiber, which are doped with e.g. rare-earth or transition metal ions. The combination of the host and the dopant creates another convenient way of categorizing lasers, e.g. Nd:YAG (neodymium dopant, yttrium-aluminum-garnet host), Ti:Sapphire, and Yb-fiber lasers.

As mentioned, fiber lasers are one branch of solid-state lasers. As explained above, the host medium is optical fiber, which has been doped by rare-earth ions. The most common dopants are ytterbium, erbium and neodymium, but e.g. bismuth, praseodymium, dysprosium, thulium and holmium have been introduced as gain fiber dopants to open up new wavelength regions. Fiber lasers have several appealing features: fiber is flexible, and can be coiled and packaged into small spaces. Moreover, the light is already in the fiber, so the output of the laser can be flexibly delivered to optical elements or the target. Active fibers have a broad gain bandwidth, which makes it possible to tune the output wavelength, and permits ultrashort pulse generation. An additional flexibility in the wavelength tuning can be realized with aid of Raman gain, a property often present in fiber-based systems (RP1). Moreover, also the absorption band is broad, so the exact pump wavelength is non-critical and the pump diode laser does not need accurate wavelength stabilization. The beam quality is great: lasers based on single-mode fiber are usually diffraction-limited, and those based on larger fibers and higher power, e.g. fiber with a 20 micron core, can also be operated with single transverse mode by bending the fiber to suppress the higher-order modes (6). Rare-earth doped fibers typically have very high gain efficiency, which enables the fiber lasers to be operated with small pump power. High gain efficiency also makes it possible to achieve high output power.

The first fiber laser, a flashlight pumped Nd-doped glass fiber laser, was realized as early as 1961 by E. Snitzer (7) in the American Optical Company. The rod-like fibers were tested in different sizes, having diameters of 32 and 305 microns. The cladding was soda-lime-silicate with an index of refraction of 1.52. The same group also developed the first fiber amplifier in 1964 (8). The fiber, having a length of 1 m, a core diameter of 10 µm and a 1.5 mm cladding, was coiled in a helical shape around the flashtube used for pumping. In 1976, J. Stone *et al.* at Bell Labs published details of a LED-pumped neodymium fiber laser (9). It was the first laser to be operated cw (continuous wave) at room temperature with a single LED pump. The advantages of the fiber geometry, the large surface to volume ratio, was noted: the laser was also the first Nd:YAG laser operating cw without a heat sink.

1.2 Pulsed lasers

Rather than continuous wave emission, many applications require the emission be modulated or pulsed. These lasers are commonly referred to as pulsed lasers. Applications of pulsed lasers are numerous in areas of optical communication, range finding, pulsed laser deposition, spectroscopy, micromachining, etc.

Pulsed operation of a laser can be realized by many different physical mechanisms depending on pulse duration, energy and repetition rate. Direct modulation is the simplest way of pulsing the laser. One can easily imagine placing a fast modulator inside the laser cavity, which allows light to escape from the cavity only for short periods of time. However, this method would result in loss of the light produced during the period when the modulator is closed. Also the modulation speed (bandwidth) of the modulator would set a lower limit for the pulse duration. There are also more sophisticated techniques for pulsing lasers, as gain switching, cavity dumping, Q-switching and mode-locking. The two latter are the most common techniques for pulsing the fiber lasers. Q-switching typically produces energetic pulses in the nanosecond range and repetition rates of a few hertz to kilohertz. In contrast, mode-locking produces shorter pulses with higher repetition rates, typically with femtosecond to picosecond duration and tens of megahertz repetition rate. Q-switching has been found a useful technique in many industrial applications, e.g. marking and other applications where high pulse energy is needed. Mode-locking is best suited to applications where extremely accurate material cutting or removal is required. For example in eye-surgery the cornea can be cut open with femtosecond pulses extremely accurately, which makes the curing more rapid and improves the quality of the cut, making the end result free of refractive errors. Both of the techniques can be further divided into active and passive techniques, depending on whether external modulation signals are used. In this thesis I have concentrated on passive Q-switching of fiber lasers by Semiconductor Saturable Absorber Mirrors (SESAMs).

1.3 Scope of this study

The goal of this thesis was to study how the parameters of SESAMs can be characterized and further refined to produce the best possible components for each purpose, be it passive mode-locking or Q-switching. The first two papers concentrate on studying and adjusting the temporal response of the SESAM structure. We developed a relatively easy technique for defining all five main parameters of a SESAM, including absorption recovery time, and studied tuning of the absorption recovery time by post-epitaxial ion irradiation and thermal annealing. In paper 3 we studied pulse width reduction of a Q-switched fiber laser to approach the physical limits using a resonant SESAM structure, and in paper 4 we studied a technique for controlling and stabilizing the pulse train of a passively Q-switched fiber laser.

2. Q-switching

Q-switching is an effective and common method for producing energetic and short (but not ultrashort) pulses. The first experimental realizations were already reported in 1961 in Hughes Research laboratories (3). In this chapter a general overview of Q-switching is given in order to understand the results presented in latter chapters.

2.1 Pulse formation in Q-switched lasers

In Q-switching pulses are produced by modulating the losses of the laser cavity. The parameter that describes how well a laser cavity can preserve its energy is the *Q-factor*, in which Q stands for the quality of the resonator. Initially, the Q-factor is kept at a low level (i.e. high losses). Constant pumping of the gain medium accumulates the spontaneous emission in the cavity. At the moment when the Q-factor is suddenly switched to a high level, spontaneous emission evolves into lasing and a laser pulse starts quickly growing in the laser cavity, which begins to deplete the gain stored in the cavity. The pulse grows stronger until the gain is equal to the losses. At that time the pulse peak power has been reached. The pulse depletes the gain wholly, the Q-switch is opened again (low Q), and the process starts from the beginning. It is beneficial for the gain material of Q-switched lasers to have a long upper-state lifetime so that the stored gain does not disappear as fluorescence emission before the Q-switch is opened (10).

As mentioned earlier, Q-switching can be realized with passive (no external modulation) or active means. Typical components for active Q-switching are acousto-optic and electro-optic modulators (AOMs and EOMs). Figure 2.1 illustrates the pulse evolution in the cavity in the case of active Q-switching. In active Q-switching the pulse appears a few round-trips after the switch is opened. In passive Q-switching the losses are self-modulated by a saturable absorber, and a pulse is formed when the gain has increased to a high enough level. In this scheme the loss modulation is not as abrupt as in active Q-switching, but the main principle is similar.

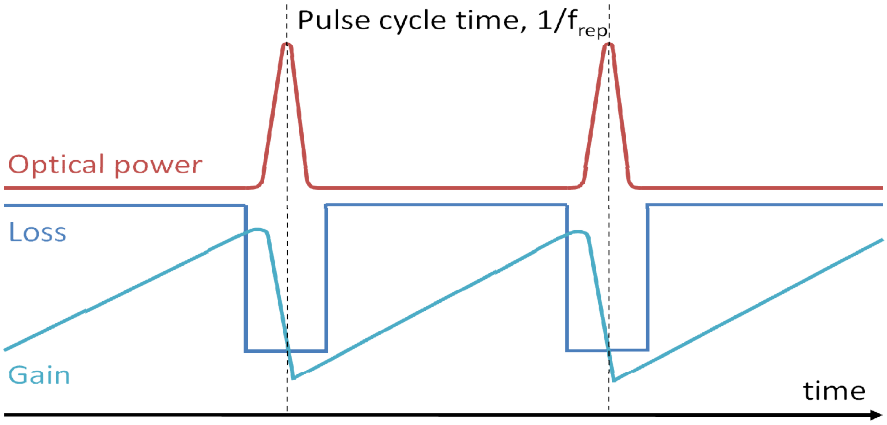

Figure 2.1: Pulse formation in active Q-switching. Pumping increases the gain while the losses are kept at a high level. When the Q-switch is opened (low-loss state) the excess gain starts building the pulse. The pulse reaches its peak when the gain is equal to the losses, after which the pulse decays.

The advantages of active Q-switching over passive are the controllable repetition rate and low timing jitter. Fundamentally, timing jitter in a Q-switched laser is inevitable because the first photon of the oscillation mode comes from spontaneous emission of the gain medium. Usually in actively Q-switched lasers the pulse width decreases and pulse energy increases with increasing pump power. The pulse width in actively Q-switched lasers has the following dependence on the gain and cavity round-trip time: $\tau_p = 8.1 \times t_{rt}/g_{rt}$, where t_{rt} is the cavity round-trip time and $g_{rt} = \ln G_{rt}$ is the round-trip gain coefficient when the pulse begins to form (11), (12). From this expression one can easily see that shortening the cavity length shortens the pulses and heavier pumping (higher gain) also reduces the pulse width. In active Q-switching the pulse energy can be increased to certain limit by reducing the repetition rate. This divides the gain to fewer pulses, so individual pulses receive higher gain. When the pulse cycle time exceeds the gain material upper-state lifetime, the amplified spontaneous emission starts to limit the pulse energy.

Conversely, passively Q-switched lasers are simpler, more cost-effective, and more compact. Q-switched microchip lasers in particular are very compact pulse sources. Usually the pulse width and pulse energy are quite independent of the pump power, but the repetition rate of a passively Q-switched laser is linearly proportional to the pump power. One weak point of the passively Q-switched lasers compared to active counter parts is the amount of timing jitter. It means the fluctuation in the timing of the pulses in the pulse train. The jitter of a passively Q-switched laser is typically in the microseconds scale and is caused by fluctuations in pump, loss, temperature etc. It is especially pronounced in fiber lasers, where there is a relatively large amount of intracavity spontaneous emission present. However, the timing jitter can be reduced by modulating or triggering the saturable absorber (P4), (13), (14) and will be discussed in Chapter 6.

2.2 Theoretical overview into Q-switching

Extensive theoretical models describing Q-switched operation have been published as early as 1963 by W. G. Wagner *et al.* from Hughes Research Laboratories (15). The topic is also broadly covered in various text books, e.g. (10) and (16).

In the paper by G. J. Spühler *et al.* (17) the authors have derived useful and fairly simple expressions for key parameters of a microchip laser passively Q-switched by saturable absorber. These results are well applicable for fiber lasers, too. Next I'm going to briefly review the expressions for pulse energy, pulse width and the repetition rate of a passively Q-switched laser.

2.2.1 Pulse energy

The expression for pulse energy is as follows:

$$E_p = E_L \Delta g \frac{l_{out}}{l_{out} + l_p} \leq E_L g_i, \tag{2.1}$$

where E_L is the saturation energy of the laser gain medium, $\Delta g = g_i - g_f$ is the gain reduction by Q-switched pulse ($g_{i,f}$ are the intensity gain coefficients just before and just after the pulse). l_{out} is the output coupling coefficient and l_p is the parasitic loss coefficient (which is usually dominated by the nonsaturable loss of the SESAM).

The pulse cycle can be divided into four phases, as shown in Figure 2.2 (17). In the beginning the absorber is in its nonsaturated state. The pulse starts to evolve when the gain has reached the level of the unsaturated value of the losses

$$g_i = l + q_0, \tag{2.2}$$

where $l = l_{out} + l_p$ and q_0 is the nonsaturated loss coefficient, i.e. the absorber in its initial state. q_0 is proportional to the modulation depth ΔR of the saturable absorber. The modulation depth is defined as the difference of the high and low intensity state reflectivities, see section 3.2. The intracavity power P starts to grow until the intensity is sufficient to saturate the absorber. The saturation energy of the SESAM is typically chosen to be at least 1 order of magnitude less than the pulse energy, so the absorber is saturated well before P reaches its maximum. Moreover, the absorber recovery time $\tau_{rec} \geq \tau_p$, so the absorber has only a minor influence on pulse development at latter phases.

In phase 2, the absorber is fully saturated, and net gain is $g = g_i - l - q \approx q_0$ since the saturable loss coefficient $q = 0$ when the absorption is completely saturated. The pulse maximum is reached when the net gain is zero, i.e. $g = l$. In phase 3 the net gain is negative and the intracavity power decreases. In phase 4 the absorber has already recovered from the saturation and the pumping of the gain to the threshold level takes place. The absorber recovery time is much shorter than the gain recovery, so the absorber is fully recovered when phase 1 starts a new cycle.

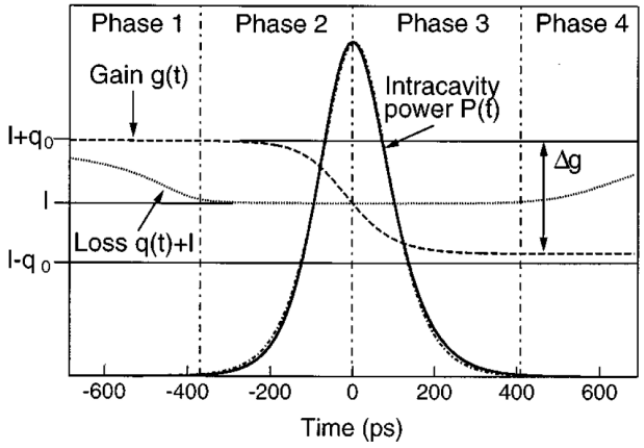

Figure 2.2: Evolution of power, loss, and gain on the time scale of the pulse width. The peak of the Q-switched pulse is reached when the gain equals the total losses (17).

The gain reduction Δg depends on q_0 and l. In most practical cases the laser is operated in the regime where $q_0 \approx l$, at which point the pulse energy is optimized and the pulse shape is nearly symmetrical. If $l \geq q_0$, the assumption $\Delta g \approx 2q_0$ is valid. Inserting Δg into Equation (2.1), we obtain the expression for pulse energy:

$$E_p \approx E_L 2q_0 \frac{l_{out}}{l_{out} + l_p} = \frac{h\nu_L}{2\sigma_L} A 2q_0 \frac{l_{out}}{l_{out} + l_p}, \text{where } q_0 \leq l. \tag{2.3}$$

In the latter expression the saturation energy E_L is expanded. In the latter form $h\nu_L$ is the photon energy, σ_L is the emission cross section of the laser material, and A is the mode area. We can increase the pulse energy by increasing the nonsaturated loss q_0 and l up to the limit set by the available gain $g_i = l + q_0$. Moreover, we have to take into account the parasitic loss l_p. When realizing pulsing with SESAMs, increasing the modulation depth (modulation depth $\Delta R \propto q_0$) usually increases the nonsaturable loss α_{ns}, too (see section 3.2 for definition). When discussing SESAM parameters instead of the quantities defined in this section, we can treat modulation depth and nonsaturated loss as synonyms. The same applies with nonsaturable loss and parasitic loss (i.e. $\Delta R \approx q_0$ and $\alpha_{ns} \approx l_p$). It has been shown in (17) that when there is some parasitic loss present, the pulse energy is optimized when the combined loss l is close to the unsaturated value of loss q_0, i.e. $l \approx q_0$.

2.2.2 Pulse width

The expression for pulse width can be formulated as follows: We can assume that the saturation energy of the absorber is small compared to the pulse energy, and thus phase 1 in Figure 2.2 has only little influence on the FWHM (full width at half maximum) of the pulse. We can further assume that in the beginning of phase 2 the gain is undepleted ($g(t) = g_i$), but the absorber is fully saturated ($q(t) = 0$). The net gain is thus $g_i - l - q \approx q_0$. In the phase 3, the net gain is $g_f - l - q = -\Delta g + g_i - l - q \approx -q_0$, since the absorber is still fully saturated ($q = 0$). This results in the growth rate and the decay rate of the Q-switched pulse both being q_0/t_{rt}, where t_{rt} is the cavity round-trip time. This leads to

an estimated FWHM pulse width of $\tau_p \approx 2\ln 2 t_{rt}/q_0$. Taking into account the decrease in growth and decay of the pulse during saturation of the gain widens the pulse by another factor of ~2, and results the expression to be the following (11), (17):

$$\tau_p \approx \frac{3.52 t_{rt}}{q_0}. \tag{2.4}$$

It should be noted that this expression gives the lower limit for pulse length achievable using a passively Q-switched laser. The pulse width of a practical laser setup might be somewhat longer due to non-ideal components etc. However, the formula indicates clearly that to shorten the pulse we need to shorten the cavity round-trip time and increase the nonsaturated loss, which in practical terms means increasing modulation depth of the saturable absorber being used.

2.2.3 Repetition rate

We can calculate the repetition rate by dividing the average output power by the pulse energy. According to (17), the average power is

$$P_{av} = \eta_s\left(P_P - P_{P,th}\right), \tag{2.5}$$

where η_s is the slope efficiency and P_P and $P_{P,th}$ are pump power and threshold pump power, respectively. The repetition rate is thus

$$f_{rep} = \frac{\eta_s(P_P - P_{P,th})}{E_p} \propto r - 1. \tag{2.6}$$

Here $r = {P_P}/{P_{P,th}}$ is the pump parameter. We can further connect the pump powers to the small-signal gain coefficient g_0 and the loss the coefficients by expressing them as (17)

$$P_P = \frac{h\nu_P A}{2\sigma_L \tau_L \eta_P} g_0, \qquad P_{P,th} = \frac{h\nu_P A}{2\sigma_L \tau_L \eta_P}(l + q_0) \tag{2.7}$$

In these expressions $h\nu_P$ is the pump photon energy, η_P is the pumping efficiency and τ_L is the upper-state lifetime of the gain medium. Inserting Eq. (2.1) and Equations (2.7) into Equation (2.6) gives us the expression for repetition rate as follows:

$$f_{rep} \frac{g_0 - (l + q_0)}{\Delta g \tau_L} \approx \frac{g_0 - (l + q_0)}{2 q_0 \tau_L}. \tag{2.8}$$

We can simplify the expression even further when operating far above the threshold by neglecting the term $l + q_0$:

$$f_{rep} \approx \frac{g_0}{2 q_0 \tau_L}, \tag{2.9}$$

because $g_0 \gg l + q_0$ when operating well above threshold.

The formulas derived in this section show the basic relations between the laser output characteristics and operation parameters.

3. Semiconductor Saturable Absorber Mirrors (SESAMs) in pulse generation

Pulsed operation in both mode-locking and Q-switching is achieved by modulating the losses of the cavity. To be more precise, the loss mechanism is referred to as saturable absorption. A saturable absorber is an optical component in which the absorption decreases when the incoming light intensity is increased. When intensity is increased to a high enough level, the absorption is fully saturated and no change in the absorption occurs if intensity is further increased. Various materials can be used as saturable absorbers in lasers: solid, dyes, and semiconductor materials. Also carbon nanotubes (CNTs) can be used as a film to act as a saturable absorber (18). This has been demonstrated by the author's group in (RP2).

Semiconductor saturable absorbers have a great advantage over other saturable absorber materials in terms of flexibility in tailoring the parameters suitable for each wavelength, gain medium and pulse form. Semiconductor manufacturing by molecular beam epitaxy (MBE) allows fine tuning of the absorption parameters.

3.1 The basic concept of SESAM

Saturable absorbers can be used both in transmission and reflection geometry. In this thesis, we have concentrated purely on the reflection scheme, in which the saturable absorber also incorporates a reflector. The component is called a *semiconductor saturable absorber mirror* (SESAM). The saturable absorber may consist of bulk semiconductor material, quantum wells (QWs) or quantum dots (QDs). Saturable absorption is a property of materials where the absorption of light decreases with increasing light intensity. In semiconductors, when the energy of a photon is equal to or exceeds the band gap energy of the material, the photon gets absorbed by the material. The absorption process can also be thought of in terms of excitation levels: an electron at the valence band gets excited by the incident photon and is lifted to the conduction band. The amount of absorption can be described by the absorption coefficient α, which describes the population at the excited and ground levels. When the excitation process is repeated at a sufficiently high pace, i.e. the intensity of the incident photons is high enough compared to the relaxation of the excitation, the valence band gets depleted, and the amount of absorption decreases. In other terms, the absorption becomes *bleached* or *saturated* at high intensities. In a two level system, the absorption can be described by the equation

$$\alpha = \frac{\alpha_0}{1 + I/I_s}, \tag{3.1}$$

where α_0 is the low intensity absorption coefficient, I the intensity and I_s the saturation intensity (19). It should be noted already at this early stage that the time response of the

absorbing material has a notable influence on the saturation intensity. The parameter that describes the temporal response of a SESAM is the *absorption recovery time*, τ_{rec}.

The mirror part of the SESAM is usually realized with a distributed Bragg reflector (DBR) grown on the semiconductor substrate. A DBR typically consists of 20–30 quarter-lambda layers of alternating high- and low refractive index materials producing over 99 % reflectivity over a band spanning more than 100 nm. The reflectivity of a DBR is based on constructive interference of reflected light at the layer interfaces. Figure 3.1 illustrates the schematics of a SESAM structure. A GaAs-based SESAM operative at a 1 µm wavelength band is used as an example here. The DBR reflector is grown first on the GaAs substrate by alternating GaAs and AlAs layers with a thickness $d = \lambda_0/4n$, where λ_0 is the operation wavelength and n is the refractive index of the GaAs or AlAs. The spacer layer is used to place the QWs at the antinode of the standing wave pattern, which is formed in the Fabry-Pérot microcavity formed between the bottom DBR and the GaAs-air interface. The semiconductor/air interface has a Fresnel-reflectivity of ~30 %. The cavity properties can be adapted by changing the reflectivity of the top surface by growing the top DBR epitaxially or by depositing a dielectric coating with the desired reflectivity post-epitaxially.

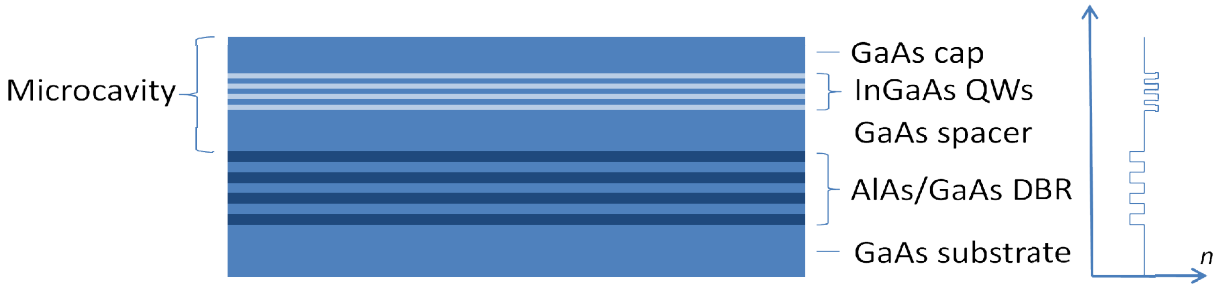

Figure 3.1: Schematic structure of SESAM working at 1 µm wavelength region along with diagram showing relative refractive indices. The microcavity is formed between the Fresnel-reflection at the surface and DBR. The GaAs spacer adjusts the QW section at the antinode of the standing wave pattern inside the microcavity.

SESAM structures can be divided into two categories depending on the microcavity properties. These two approaches are *antiresonant* and *resonant*, depending on whether the resonance wavelength of the cavity is matched to the operation wavelength λ_{op} (*resonant*) or mismatched from λ_{op}. The matching is applied when the optical length of the microcavity L ($L = \Sigma n_i d_i$ for each layer) is an integer multiple of λ_{op}. The resonance properties have a great impact on the device operation in a laser cavity. For example, the two-photon absorption (TPA) effect which is useful for preventing Q-switched mode-locking (QSML) can be tuned by changing the reflectivity of the top mirror (RP3).

In general, resonant structures have higher nonlinearity than anti-resonant ones. In resonant structures incident light makes multiple roundtrips through the QWs in microcavity, which leads to higher absorption. As mentioned earlier, the absorption is usually also enhanced by placing the QWs at the antinode of the standing wave pattern in the microcavity. The desired amount of absorption depends on the laser characteristics in

which the absorber is used. Fiber lasers can tolerate higher loss due to high gain, and thus high modulation depth can be applied. In fiber lasers significant modulation depth (over 10 %) is needed for initializing mode-locking or Q-switching. On the other hand, Vertical-external-cavity surface-emitting lasers (VECSELs) have low single-pass gain which makes the cavity extremely sensitive to loss. In such lasers it is compulsory to limit the modulation depth to low values, ΔR ~ 1 % (RP4).

3.2 SESAM characteristics

SESAM performance is characterized by four parameters:

i) Modulation depth ΔR
ii) Saturation fluence F_{sat}
iii) Nonsaturable loss α_{ns}
iv) Recovery time of absorption τ_{rec}

The three first parameters are illustrated in Figure 3.2. The plot shows average reflectivity as a function of incident pulse fluence (fluence=pulse energy per mode area). Average reflectivity means that the reflectivity is measured as a ratio between incoming and reflected average power in a macroscopic time scale, not reflectivity changes in picoseconds time scale. Modulation depth is defined as the difference between low-intensity reflectivity R_{linear} and high-intensity reflectivity R_{ns}. The fluence at which the 1/*e* value of ΔR is achieved is called the saturation fluence F_{sat}. The difference between perfect reflectivity ($R = 1$) and high-intensity reflectivity R_{ns} is the nonsaturable loss α_{ns}.

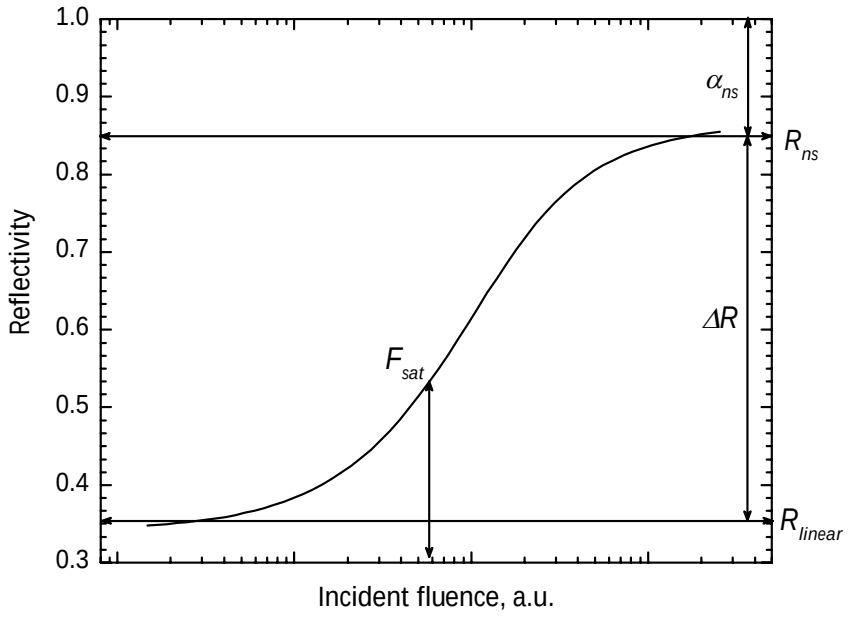

Figure 3.2: Nonlinear reflectivity curve of a high-modulation depth SESAM. The reflectivity of the SESAM has been measured as a function of incident pulse fluence. The figure illustrates the parameters ΔR, F_{sat}, and α_{ns}.

The nonlinear reflectivity of a SESAM can be expressed as a function of incident pulse fluence F (20):

$$R(F) = R_{ns} - \left[1 - \exp\left(-\frac{F}{F_{sat}}\right)\right]\frac{\Delta R}{F/F_{sat}}. \quad (3.2)$$

This equation makes the assumption that the incident pulse width is shorter than the absorption recovery time ($\tau_p < \tau_{rec}$). The nonlinear reflectivity measurement details are discussed in more detail in section 3.3.

Absorption recovery time τ_{rec} can be determined with several techniques. The two most common techniques are the pump-probe technique (21) and time-resolved photoluminescence using a femtosecond up-conversion method (22). These, however, require sophisticated and expensive equipment. Therefore we developed a simple technique for τ_{rec} determination. This technique is described in more detail in subsection 3.3.3. Absorption recovery time is a very important parameter of a SESAM. It very much determines device suitability for a desired pulsing technique (Q-switching, mode-locking, Q-switched mode-locking). SESAMs can be divided roughly into two categories, fast and slow. Moreover, the absorption recovery has a bi-temporal response. In a high lattice quality semiconductor the dominant absorption recovery process has a lifetime of few nanoseconds determined by the radiative carrier-recombination time (23). In order to obtain stable and reliable mode-locking operation, the absorption recovery has to also include shorter components. This is usually realized by introducing defects in the lattice, which act as non-radiative recombination centers with short recovery time. There are several techniques for realizing fast recovery times in a semiconductor structure via the introduction of defects in a controllable manner, including

- Low-temperature growth (24), (25), (26)
- Doping the active region (25), (26), (27)
- Ion irradiation/implantation (28), (29)
- Proton bombardment (30), (31)
- Surface state free-carrier trapping (32)
- Metamorphic growth (33), (34)
- Band-gap engineering (35).

Each of the aforementioned methods has their pros and cons, which are creditably summarized in S. Suomalainen's doctoral thesis (36). In (P2) we studied absorption recovery time reduction by Ni-ion irradiation and thermal annealing.

3.3 Measuring the nonlinear response in different operation regimes

As mentioned in the previous section, the temporal response and saturation fluence are key characteristics of saturable absorbers. It is generally expected that the nonlinear reflectivity of a SESAM depends on the duration of the incident pulse. Particularly, when the pulse

width becomes significantly larger than the absorption recovery time, a higher pulse energy is needed to saturate the absorption. It has also been shown that quasi-cw amplified spontaneous emission can degrade significantly the nonlinear response of a SESAM (37). SESAMs with a fast nonlinear response are, however, less affected by the cw radiation. It is important that the SESAM nonlinear response is characterized with the pulse duration and wavelength similar to the conditions when the absorber mirror operates in a laser. The correct absorber parameters can then be used in a laser simulation to estimate the steady-state output pulse characteristics. Unfortunately, when the SESAM parameters are discussed in the literature, the pulse width used in the measurements is seldom mentioned. In the following, the dependence of the nonlinear response of a saturable absorber depends on the parameters of the optical pump pulses is shown.

3.3.1 Experimental setup

In this work an experimental setup for measuring the nonlinear response of a SESAM has been developed. The setup consists of 3 units, which are illustrated in Figure 3.3:

i) Pulse source:

The gain fiber is pumped with a fiber coupled laser diode (LD). The laser cavity is formed between the SESAM and a fiber loop mirror.

ii) Amplifier:

The pulse fluence is amplified in a fiber amplifier. Two isolators precede and follow the amplifier, preventing unwanted back reflections from disturbing the signal.

iii) Measurement unit:

The output from the fiber is collimated and divided into two with a beam splitter cube. The reflected and reference signals are monitored with a dual-channel power meter.

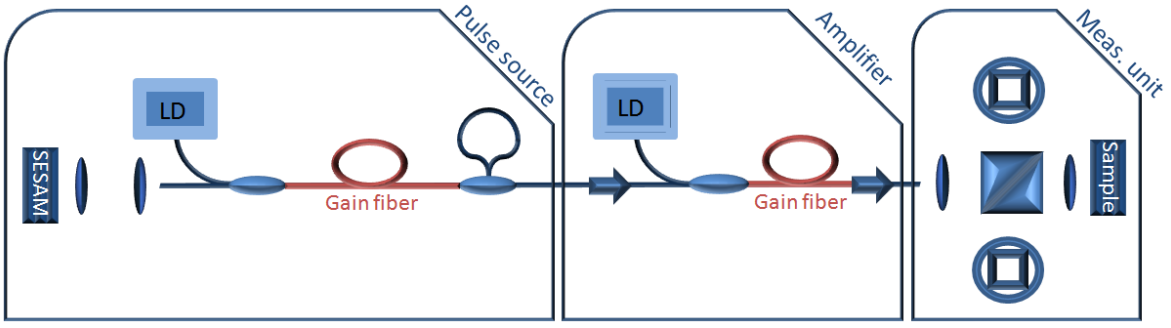

Figure 3.3: A schematic illustration of the experimental setup for nonlinear reflectivity measurements.

The pulse source has in most cases been either a mode-locked or Q-switched fiber laser, depending on the operation regime of the sample. A mode-locked oscillator operating at the

1 µm spectral range needs a dispersion compensation element, e.g. a grating pair or a dielectric thin film Fabry-Pérot etalon (RP5), to compensate the fiber dispersion, which is omitted from the figure for illustrative purposes. Also, a polarization controlling element is frequently used in the cavity. The pulse fluence straight from the oscillator is usually insufficient to saturate the sample, so the pulse train is typically amplified in the fiber amplifier. The output from the amplifier is led to the measurement unit, in which the amplitude of the pulses is adjusted by a variable 30-dB attenuator (not shown in the figure). The output is divided into two beams by a polarization independent beam splitter cube. One beam is focused on the sample by a microscope objective and the other serves as a reference for the incident pulse fluence. The focused beam radius on the absorber is measured using the knife-edge technique and is typically a few microns. The intensities of the beams are detected by a dual-channel power meter. The average reflectivity of the SESAM is determined by the ratio between the reflected beam and the reference beam. The ratio is then plotted against the incident fluence, which can be calculated from the reference beam. This data is then fitted to Equation (3.2), from which $\Delta R, F_{sat}$, and α_{ns} can be extracted.

To study the saturation behavior with different pulse characteristics, the nonlinear reflectivities of a slow and a fast SESAM have been measured with different pulse widths: 29 ps, 1.5 ns, 6 ns, 10 ns and 20 ns. The 29 ps pulse source was a mode-locked erbium fiber laser having a repetition rate of 14.5 MHz. The emission wavelength was 1553 nm. The nanosecond pulses were obtained from a distributed feedback (DFB) laser diode modulated by a signal generator and a pulse pattern generator. The repetition rate and emission wavelength of the pulse train in the case of the nanosecond pulses were also set to 14.5 MHz and 1553 nm. The pulse shape of the nanosecond pulses was close to square due to the typical rise/fall time of the DFB laser of 0.2 ns. The signal from the DFB laser was amplified in two stages. The amplified spontaneous emission was filtered out between the amplifier stages and from the output by bandpass filters.

The absorber under study has been successfully used for mode-locking erbium fiber laser (38), (39). The absorber mirror comprises 28 9-nm-thick InGaAs quantum wells grown monolithically by molecular beam epitaxy on a highly-reflective distributed Bragg reflector. The SESAM has been tested in two versions – the slow absorber was as-grown; the fast one was post-growth irradiated with heavy ions. Irradiation with 10-MeV Ni-ions with a dose of $10^{11}/cm^2$ was expected to reduce the recovery time of absorption from the nanosecond range to the picosecond-range (29). The effective saturation fluence experienced a notable increase when increasing the pulse width from 29 ps to 6 ns, especially in the case of the fast SESAM. The measurement results from the fast SESAM are summarized in Figure 3.4. These results, together with data obtained for the slow SESAM were used to derive the absorber recovery times with the method described in subsection 3.3.3.

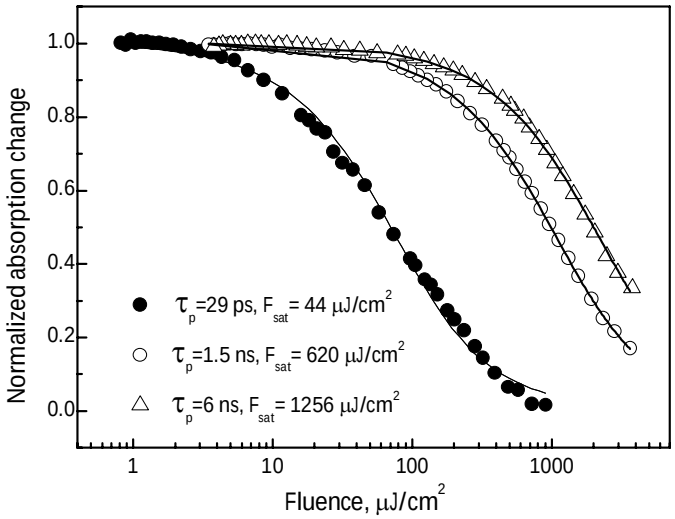

Figure 3.4: Normalized absorption change measured as a function of pump pulse fluence. The data have been obtained with 29 ps, 1.5 ns and 6 ns-long pulses from a fast saturable absorber mirror.

3.3.2 Absorber model

Saturable absorber was modeled using the rate equation (40)

$$\frac{dq(t)}{dt} = -\frac{q(t) - q_0}{\tau_{rec}} - \frac{qI(t)}{F_{sat}}, \tag{3.3}$$

where $q(t)$ is absorber saturable loss, q_0 is the nonsaturated loss, τ_{rec} the recovery time, F_{sat} the saturation fluence for pulses much shorter than the absorber recovery time, and $I(t)$ is the incident intensity. The model does not take into account femtosecond scale behavior from fast thermalization, carrier cooling etc. but since we study picosecond and nanosecond regimes here, we can safely ignore faster phenomena. An analytical solution of the inhomogeneous linear differential equation (Eq. (3.3)) can be derived assuming constant incident intensity during the pulse width, i.e. assuming square-shaped pulses:

$$q(t + t_0) = \left[q(t_0) - \frac{q_0 F_{sat}}{F_{sat} + I\tau_{rec}}\right] * \exp\left[-\left(\frac{1}{\tau_{rec}} + \frac{I}{F_{sat}}\right)t\right] + \frac{q_0 F_{sat}}{F_{sat} + I\tau_{rec}} \tag{3.4}$$

where $q(t_0)$ is the initial saturable loss at the time t_0. A square-shaped pulse with fluence F_p and duration τ_p experiences a fluence loss ΔF_p at reflection from the SESAM:

$$\Delta F_p = \int_{t_0}^{t_0+\tau_p} \frac{F_p}{\tau_p} q(t + t_0) dt. \tag{3.5}$$

Let's define normalized saturable loss l by normalizing the fluence lost to the nonsaturated loss:

$$l = \frac{\Delta F_p / F_p}{q_0}. \tag{3.6}$$

We can calculate normalized saturable loss by substituting Equations (3.4) and (3.5) into Eq. (3.6):

$$l = \frac{1}{\frac{F_p}{F_{sat}}\left(1+\frac{F_{sat}}{F_p}\frac{\tau_p}{\tau_{rec}}\right)^2}\left[1 - e^{-\frac{F_p}{F_{sat}}-\frac{\tau_p}{\tau_{rec}}} + \frac{\tau_p}{\tau_{rec}} + \frac{F_{sat}}{F_p}\frac{{\tau_p}^2}{{\tau_{rec}}^2}\right]. \tag{3.7}$$

Normalized saturable loss as a function of pulse fluence has been plotted for different pulse durations in Figure 3.5. Both the experimental results presented in Figure 3.4 and the modeling results presented in Figure 3.5 confirm that higher fluence is needed to saturate the absorber with a pulse of longer duration. For long pulses or very fast absorbers ($\tau_p \gg \tau_{rec}$) we can simplify and solve Eq. (3.7) for normalized pulse fluence F_p/F_{sat}

$$\frac{F_p}{F_{sat}} = \frac{1}{2l} + \frac{\tau_p}{\tau_{rec}}\frac{1-l}{l}. \tag{3.8}$$

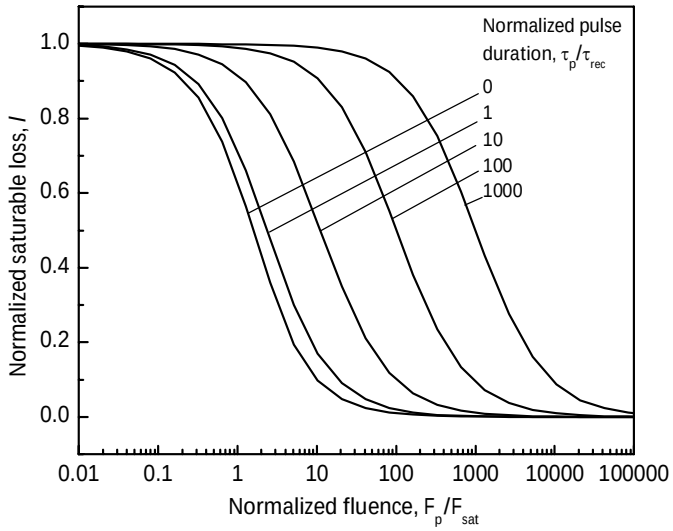

Figure 3.5: Normalized saturable loss l as a function of incident fluence plotted for different pulse durations. The saturable loss has been normalized to modulation depth, incident pulse fluence to saturation fluence, and pulse duration to absorption recovery time.

To quantify the change in the nonlinear response of the saturable absorption as the pulse width is varied, we define here an effective saturation fluence $F_{sat,eff}(\tau_p)$, which is the pulse fluence F_p at which the normalized saturable loss l drops by a factor of $\frac{1}{(1-1/e)}$. With this definition, we get the dependence

$$\frac{F_{sat,eff}}{F_{sat}} \propto s\frac{\tau_p}{\tau_{rec}}, \tag{3.9}$$

where the slope s is 0.58 for square-shaped pulses. By solving the (3.3) numerically, s for Gaussian and sech^2 pulses has been found to be 0.94 and 1.09, respectively.

3.3.3 A simple method for absorption recovery time determination

As mentioned in section 3.2, the absorption recovery time can be measured by e.g. time-resolved photoluminescence or a pump-probe setup. Performing those sophisticated measurements is not always possible due to time or resource limitations. A simple method for determining the absorption recovery time from nonlinear reflectivity data has been developed.

First, to determine the absorber recovery time τ_{rec}, the effective saturation fluence $F_{sat,eff}$ has to be measured with pulses longer than absorption recovery time, preferably with several pulse widths. Saturation fluence F_{sat} should be measured with short pulses ($\tau_p < \tau_{rec}$), too. The ratio $\frac{F_{sat,eff}}{F_{sat}}$ is plotted as a function of pulse width τ_p. Absorber recovery time can then be derived by comparing the slope of $\frac{F_{sat,eff}}{F_{sat}}$ to the slope s of Eq. (3.9), taking into account the shape of the long pulses used in the measurement. In Figure 3.6 the experimental data and linear fits are plotted for the fast and slow absorbers discussed above. The recovery times are 120 ps and 1.0 ns, respectively. This is in good agreement with pump-probe measurements and literature references.

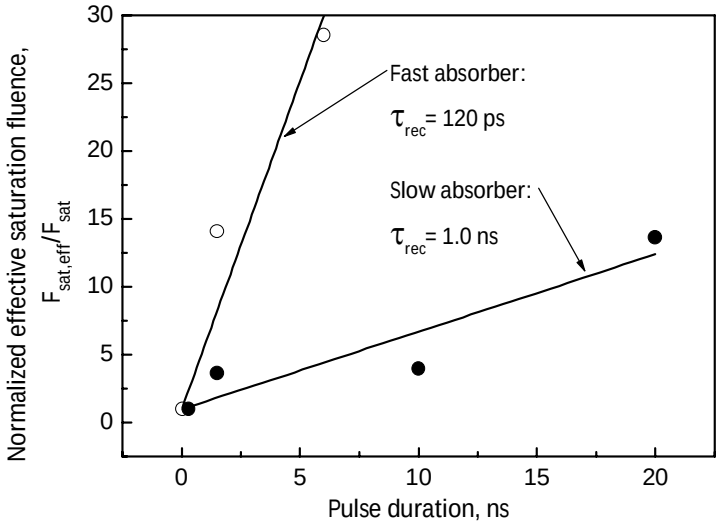

Figure 3.6: Measured normalized effective saturation fluence as a function of pulse duration used in the measurements plotted for a fast ion-irradiated and slow as-grown SESAM.

3.4 Adjusting the recovery time

In Chapter 3.2 the different methods for shortening the absorption recovery time were listed. In (P2) we studied a combined method of Ni-ion irradiation and rapid thermal annealing (RTA) in order to achieve more flexibility in absorption recovery times – not just "slow" recovery of as grown sample and "fast" recovery of irradiated SESAM. Moreover, the effect of absorption recovery time on other parameters, especially on effective saturation

fluence and effective modulation depth was under study. Thermal annealing also improves the temporal stability of SESAM parameters, being based on the removal of short-lived defects. The samples were irradiated with 6 MeV Ni-ions with a dose of 5×10^{11} /cm^2 and annealed with different temperatures and recipes. The nonlinear properties of the samples were characterized by measuring nonlinear reflectivity with different pulse durations, and finally their pulsing properties were tested by placing the samples into fiber laser cavity.

The samples had 30.5 pairs of AlAs/GaAs layers forming a highly reflective DBR, followed by the absorber section of 3 InGaAs QWs separated by 20 nm thick barriers. On top of the absorber 60 nm of GaAs was grown as a cap layer. Annealing of the irradiated samples was performed in a dry nitrogen atmosphere with a protective SiO_2 film deposited by plasma enhanced chemical vapor deposition (PECVD) on the sample prior to annealing to prevent outdiffusion. The ramp-up rate from room temperature to the annealing temperature was 5.5 °C/s. The protective film was etched away after thermal treatment. The annealing was performed at temperatures of

- 400 °C for 30 s,
- 400 °C for 60 s
- 400 °C for 120 s, and
- 600 °C for 30.

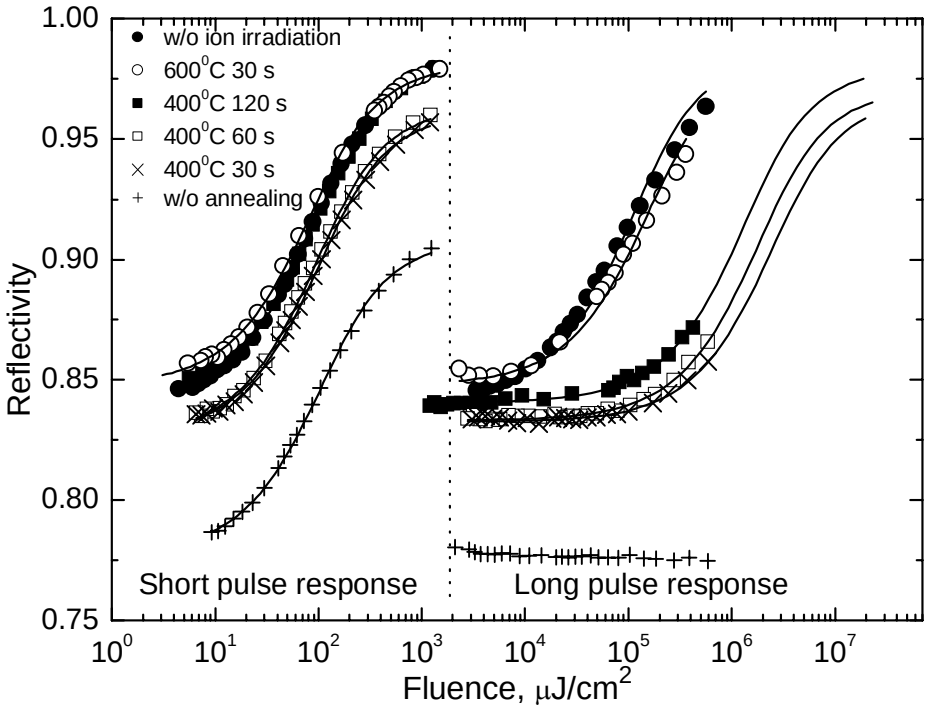

Figure 3.7: The nonlinear reflectivity measured as a function of pulse fluence. The short and long pulse response of the samples has been measured using 2 ps and 370 ns pulses as probe signals, respectively.

Figure 3.7 shows the nonlinear reflectivity response of the slow as-grown sample and the fast ion-irradiated sample having undergone different recipes of thermal annealing. The

short pulse response was studied using a mode-locked fiber laser with a pulse duration of 2 ps, and the long pulse response using a Q-switched fiber laser with a pulse duration of 370 ns. We can conclude from Figure 3.7 that the modulation depth is fairly independent of the ion irradiation and thermal annealing and remains at ~14 % throughout the studies. In Figure 3.7 one can clearly see a rise in the effective saturation fluence $F_{sat,eff}$ when comparing the results measured with short and long pulses. Another conclusion that can be derived from Figure 3.7 is that with appropriate thermal annealing (600 °C, 30 s), the effect of ion irradiation can be largely eliminated and the parameters of the absorber can be restored, resulting in values typical for an as-grown slow sample observed prior to ion irradiation. Annealing therefore allows the recovery time and, consequently, the effective saturation fluence of the absorption to be set at any value ranging from the characteristic values for fast (after ion irradiation) and slow (as-grown) absorber mirrors. The plots in Figure 3.7 also illustrate that when absorption recovery time reduces, saturation of the absorber become progressively difficult, especially with long Q-switched pulses. The effective modulation depth for long pulses is therefore only a fraction of the modulation depth for short pulses, leaving high nonsaturable losses. In particular, the ion-irradiated fast absorber without thermal annealing shows no sign of saturation at the long pulse regime on the right hand side of Figure 3.7.

Absorption recovery time τ_{rec} was extracted from the nonlinear reflectivity measurement data with the method described in section 3.3.3. The results are listed in Table I, which also shows the regime of laser operation when the sample is placed in the fiber laser cavity acting as a test bed. Figure 3.8 plots (filled circles) effective saturation fluence determined from the measurements with a Q-switched laser source (τ_p=370 ns) as a function of the absorption recovery time. This illustrates the increase in effective saturation fluence with the increase in the speed of the absorption recovery. The experimental data is well in line with simulated data (half-filled circles) that has been extracted by solving Eq. (3.3) numerically for pulses with different durations and energies. The solid line presents the fit using the expression $F_{sat,eff}/F_{sat,\tau\to 0} = 0.94\tau_{pulse}/\tau_{rec}$ (Eg. (3.9)) using τ_{pulse}=370 ns.

Another essential though expected feature is the decrease in nonsaturable losses with thermal annealing, which is illustrated in the same plot (with empty circles) as a function of absorption recovery time.

Table I: Effect of Ni-ion irradiation and thermal annealing on absorption recovery time and laser operation.

Annealing parameters	Recovery time (ps)	Laser operation
As-irradiated	2	Self-starting of mode-locking is critical
400 °C, 30 s	9	Excellent, robust starting of mode-locking
400 °C, 60 s	11	Good starting of mode-locking
400 °C, 120 s	15	Starting mode-locking is difficult, double pulses
600 °C, 30 s	119	Q-switching with some instability
As-grown	170	Stable Q-switching

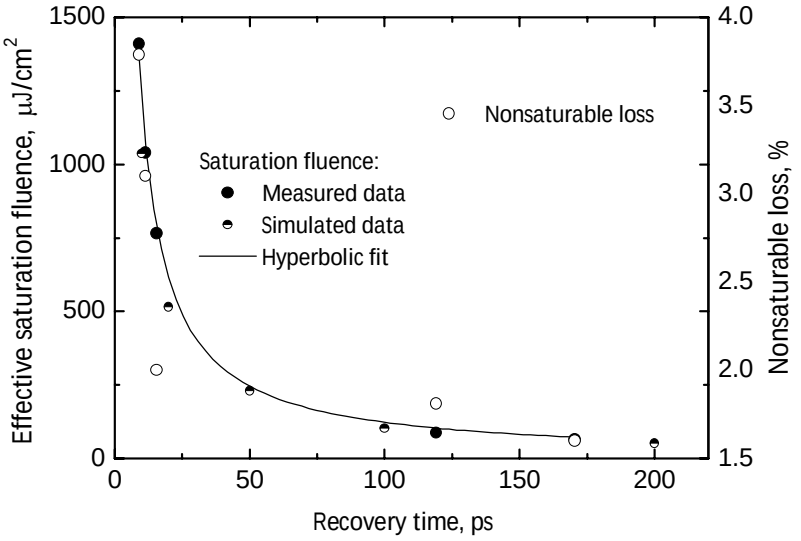

Figure 3.8: Effective saturation fluence plotted versus absorption recovery time. The pulse width used in the measurements (filled circles) and simulation (semi-filled circles) is 370 ns. The nonsaturable loss (empty circles) extracted from the nonlinear reflectivity measurements is also plotted on the right hand side axis.

As a conclusion from the results listed above, a combined method of Ni-ion irradiation and thermal annealing proved to be an efficient method of tailoring absorber parameters from values corresponding to the slow as-grown absorber to those obtained using high-energy heavy ion irradiation. Different operation regimes of a pulsed laser could thus be achieved with the same semiconductor structure depending on the regime of the postgrowth processing. In addition, thermal annealing decreases the nonsaturable losses and is expected to have a positive impact on the long-term operation due to the removal of the short-lived states induced by ion irradiation.

4. Design drivers of SESAM for Q-switching

We discussed in section 2.2 the laser parameters that affect the pulse energy, pulse width and repetition rate of a Q-switched laser. In order to optimize the output of the laser, the saturable absorber has to be designed according to these guidelines. In section 2.2 we reached the conclusion that the pulse energy is optimized when the nonsaturated loss q_0 are close to the overall cavity losses. However, the available gain has to overcome the overall losses, naturally. The advantageous features of fiber lasers include high gain – even a straight cleave at the end of the gain fiber giving a ~4 % back reflection provides enough feedback to initialize lasing.

On the other hand, the higher the nonsaturated loss q_0, the shorter the output pulse width. When discussing SESAM parameters, we can treat nonsaturated loss and modulation depth ΔR as synonyms. In order to achieve short and energetic pulses from a passively Q-switched fiber laser, the modulation depth should be high, tens of percents. Nonsaturable loss α_{ns} should be minimized. However, high modulation depth usually brings some nonsaturable loss along as a trade off.

4.1 High modulation depth

Increasing modulation depth means increased absorption. This can be achieved for example by increasing the number of quantum wells. However, increasing the number of QWs may raise the saturation fluence to a level that cannot be achieved in the cavity. In practical terms, this means that the effective modulation depth is lower and an additional loss is observed, because high reflectivity state R_{ns} cannot be reached. Therefore, a way to achieve high modulation depth while maintaining moderate saturation fluence is to design the SESAM such that the QWs are in a resonant Fabry-Pérot cavity. Such devices are frequently referred to as *resonant SESAMs.* The resonance effect can be further enhanced by placing the QWs at antinodes of the standing wave pattern formed.

The reflectivity of a resonant SESAM can be expressed with the Fabry-Pérot model (10):

$$R = \frac{\left(\sqrt{R_T} + \exp(-2\alpha d)\right)^2 - 4\sqrt{R_T}\exp(-2\alpha d)\cos^2\left(\frac{\Phi_{rt}}{2}\right)}{\left(1 + \sqrt{R_T} + \exp(-2\alpha d)\right)^2 - 4\sqrt{R_T}\exp(-2\alpha d)\cos^2\left(\frac{\Phi_{rt}}{2}\right)}, \tag{4.1}$$

where R_T is the top mirror reflectivity, α is the absorber amplitude absorption coefficient, d is the cavity thickness, and Φ_{rt} the round-trip phase shift in the cavity. The phase shift consists of the following components (41):

$$\Phi_{rt} = 2n_{eff}kd + \Phi_b + \Phi_t, \tag{4.2}$$

where n_{eff} is the refractive index of the cavity layers, $k = 2\pi/\lambda$ the wave number, d the physical thickness of the cavity, and $\Phi_b$and Φ_t are the phase shifts from the bottom and top mirrors, respectively. In the model the bottom mirror reflectivity is considered to be 100 %.

The SESAM structure is resonant if $\Phi_{rt} = 2m\pi$, and antiresonant if $\Phi_{rt} = (2m+1)\pi$. Assuming the sum of the phase shifts from bottom and top mirrors to be 2π, which is usually the case in SESAMs where additional coatings haven't been applied, the optical thickness of the cavity L is

$$L = n_{eff}d = \frac{\Phi_{rt}}{2k} = \begin{cases} \frac{m\lambda}{2} & \text{(resonant)} \\ \frac{(2m+1)\lambda}{4} & \text{(antiresonant)} \end{cases}. \tag{4.3}$$

The optical properties of the SESAM can be varied greatly by the thickness of the cavity. In particular, modulation depth is strongly enhanced and saturation fluence reduced if we compare the values of a resonant SESAM to an anti-reflection coated (AR) SESAM. The field intensity in the resonant SESAM microcavity is enhanced by a factor ε compared to the intensity of an AR-coated (cavity-free) structure I_0 (42):

$$I = \varepsilon I_0, \tag{4.4}$$

where

$$\varepsilon = \frac{1 - R_T}{\left(1 + \sqrt{R_T}\exp(-2\alpha d)\right)^2 - 4\sqrt{R_T}\exp(-2\alpha d)\cos^2\left(\frac{\Phi_{rt}}{2}\right)}. \tag{4.5}$$

At the same time the effective saturation fluence is reduced by a factor 1/ ε:

$$F_{sat,eff} = \frac{1}{\varepsilon}F_{sat,0}. \tag{4.6}$$

The modulation depth of a resonant absorber can reach 100 % with an impedance matched microcavity design (43). The low-intensity reflectivity spectrum of a highly resonant SESAM with very high modulation depth is seen in Figure 4.1. The nonlinearity of the as-grown SESAM has been further enhanced by evaporating a dielectric coating having a reflectivity of 60 % on the top of the SESAM, leading to a nearly impedance matched microcavity.

Resonant SESAMs have proved to be efficient in producing high modulation depths for Q-switched lasers. In mode-locked lasers, the resonant properties of SESAMs can also be used to find the optimal characteristics for ultra-short pulse operation. In (RP3) the enhancement of saturable and two-photon absorption (TPA) in resonant SESAMs was studied. By proper design of the resonant structure the enhanced TPA can effectively prevent unwanted Q-switched mode-locking (QSML) when operating in the mode-locked regime, whilst maintaining the high modulation depth required for self starting of the mode-locking.

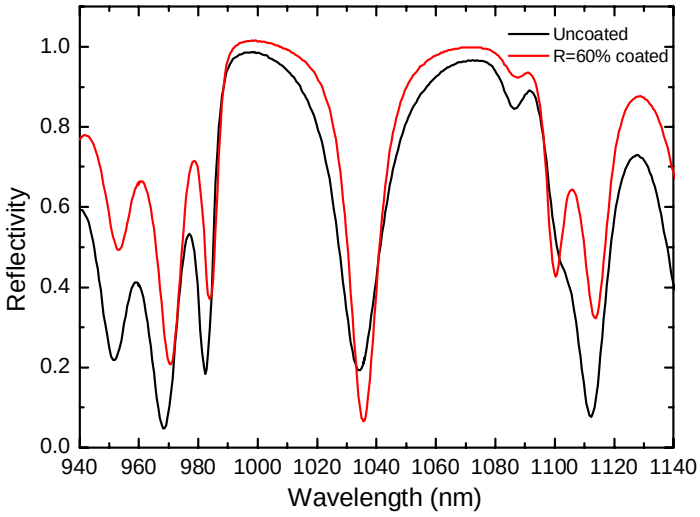

Figure 4.1: Low-intensity reflectivity spectrum of a highly resonant SESAM. The resonance properties of the uncoated SESAM have been further tuned by evaporating a dielectric coating having ~60% reflectivity on the top of the SESAM leading to a nearly impedance matched structure. Courtesy of RefleKron Ltd.

4.2 Time response

It has been shown that the reduction in absorption recovery time τ_{rec} does not notably affect the pulse duration of a passively Q-switched laser (11), (12). Actually, fast saturable absorbers may cause additional losses for long Q-switched pulses when the pulse width is significantly longer than the absorption recovery time. The upper limit for the absorption recovery time is the pulse-to-pulse duration of the Q-switching pulse train (44),

$$\tau_p < \tau_{rec} < \frac{1}{f_{rep}}. \tag{4.7}$$

Therefore, the optimal time response of a SESAM for Q-switching a fiber laser should be at the nanoseconds scale.

The condition for effective passive Q-switching assuming an adiabatic response of the saturable absorber (10), has been given in (45), (46)

$$\frac{E_g}{E_a} > \frac{1}{2q_0}\frac{t_{rt}}{\tau_{rec}}, \tag{4.8}$$

where the ratio of the saturation energies of gain material and absorber, respectively, is on the left side. The saturation energy of the gain fiber is typically fairly high, e.g. a 6-micron core ytterbium fiber has a saturation energy of 5 µJ (47). This corresponds to saturation fluence (energy per area) of 17.7 J/cm^2. This is many times higher than the saturation energy of the absorber. E.g. in (P3) the saturation fluence of the absorber for 10 ns pulses is 5 mJ/cm^2. It should be emphasized that the saturation fluence of the absorber depends strongly on the pulse length, as is shown in (P1). Again, the roundtrip time in (P3) is 2.5 ns, the modulation depth is ~0.7 and the recovery time ~1 ns. The left side of the equation then

has a value of 3540, whereas right side is 1.79. Therefore, high saturation of the gain is generally not a limiting factor in Q-switched fiber lasers where the requirement for absorption recovery time is mainly determined by the laser efficiency which intuitively suggests that recovery time should be close to the pulse length.

Long, ~1 ns recovery time is usually achieved by high-quality lattice growth by solid state molecular beam epitaxy (SS-MBE). R. Paschotta *et al.* report even longer, 13 ns recovery time of a SESAM used for Q-switching a fiber laser at 1.53 µm (48). The SESAM was grown with metal-organic chemical vapor deposition (MOCVD) on an InP substrate. The absorber section is bulk $In_{0.58}Ga_{0.42}As_{0.9}P_{0.1}$ and lattice matched to InP. The absorber section is capped with an InP-layer to prevent lifetime reduction by surface recombination of carriers. S.C. Huang *et al.* claim to have over 100 ns relaxation time for a transmission SESA based on AlGaInAs quantum wells (49). Unfortunately they don't specify the characterization method.

However, one possible topic for further research would be developing a QW-based SESAM having several nanoseconds recovery time.

5. Approaching short-pulse Q-switching

As the pulse width of a Q-switched laser is proportional to the cavity round-trip time (11), the fiber laser cavity length typically sets the limitation on the achievable pulse width. With other technologies, e.g. microchip lasers, picosecond pulses have been realized (50). Thus, parameters other than the cavity length must be taken under study in order to shorten the pulse. In (P3) we produced 8-ns pulses from a passively Q-switched ytterbium fiber laser by increasing the modulation depth ΔR of the absorber. The pulses were at the date of writing (P3) the shortest obtained from a passively Q-switched fiber laser, which gained attention from Nature Photonics (51). Sub-10 ns pulses generated by actively Q-switched fiber lasers have been reported by several groups: In 1992 P. R. Morkel *et al.* already reported 2 ns pulses with a short, high-gain, compound-glass fiber and a fast, high-extinction electro-optic modulator (52). J. Limpert *et al.* reported 7.0 ns pulses with energy 0.5 mJ from Yb-doped photonic crystal fiber and a BBO Pockels-cell together with a thin film polarizer (53). O. Schmidt *et al.* report 7.3 ns and 2 mJ pulses generated by a rod-type Yb-fiber laser modulated by acousto-optic modulator (54). However, to the best of my knowledge, the 8 ns pulses published in (P3) are still the shortest from passively Q-switched fiber laser.

5.1 8 ns pulses with a resonant SESAM

A resonant Fabry-Pérot structure in a SESAM microcavity proved to be an efficient way to increase the modulation depth of the absorber, as discussed in Chapter 4.1. In antiresonant geometries the modulation depth can be increased by increasing the number of quantum wells, but this makes saturating the absorber difficult, i.e. it increases the saturation fluence. A resonant geometry helps to keep the saturation fluence at a reasonably low level since the incident pulse makes several roundtrips in the microcavity. Moreover, we shortened the cavity using highly doped fiber as a gain medium and using dichroic coated fiber as an input coupler / end mirror. The fiber laser cavity is formed between the lens coupled SESAM and a polished fiber connector, which has a dichroic coating with a reflectivity of 65% at 1050 nm and is highly transparent at the pump wavelength (55). The 15 cm Yb-doped gain fiber, having an absorption of 2000 dB/m at 980 nm, was core pumped at 974 nm through the coated connector by a laser diode. The maximum absorbed pump power was 125 mW. A thin Fabry–Pérot etalon was placed into the free-space section of the cavity to control the operation wavelength. Throughout the experiments, a short piece of passive single-mode (Flexcore 1060) fiber could be spliced to the gain fiber to study the effect of cavity length on the Q-switched pulse duration. The cavity round-trip time was first set to 13 ns and then decreased to 2.5 ns by removing the passive (undoped) fiber from the laser cavity.

The SESAM used in this study was fabricated by solid-source MBE on n-type GaAs(100) substrate. The sample includes a bottom mirror comprising 24 pairs of AlAs/GaAs quarter-wave layers forming a distributed Bragg reflector (DBR). The DBR's stop band had a center wavelength of 1050 nm and a 120 nm bandwidth. The absorber section comprises 14 InGaAs quantum wells with 8 nm thickness. The quantum-well structure is sandwiched between a GaAs buffer layer and a 100 nm GaAs cap layer. The thickness of the buffer layer was adjusted to the resonance condition of the Fabry–Pérot microcavity formed by the semiconductor DBR and the top reflector at the semiconductor/air interface.

The low-intensity reflectivity spectrum of the SESAM used in this study, shown in Figure 5.1, reveals the deep resonance dip resulting in a high modulation depth of 70 % at the wavelength of 1043 nm. The modulation depth is listed also at a few other wavelengths marked in the figure.

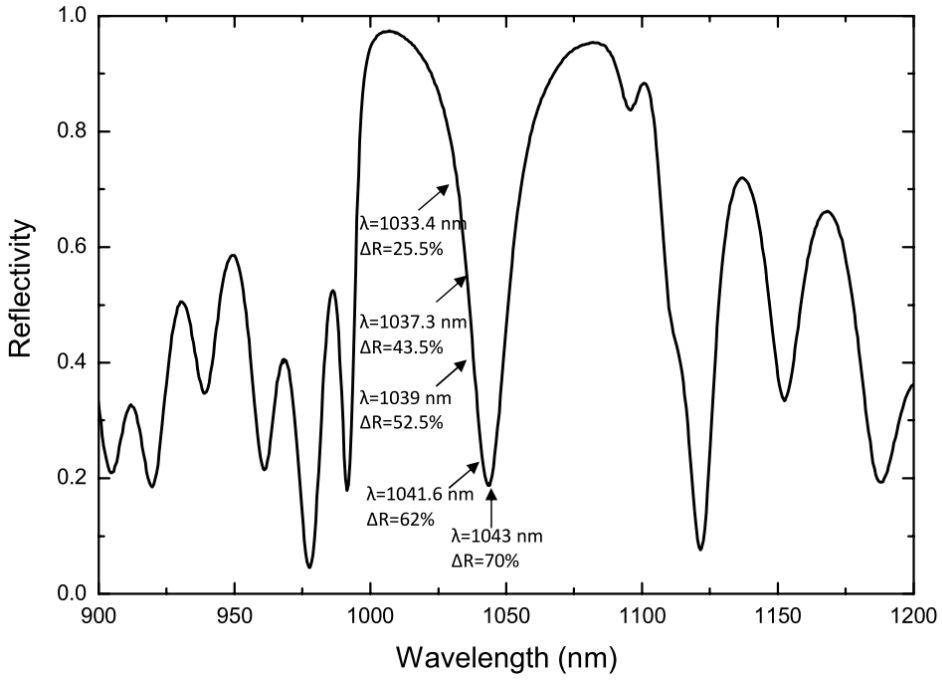

Figure 5.1: Low-intensity reflectivity spectrum of the resonant SESAM used in experiments. Modulation depth ΔR has been listed at a few wavelengths.

The performance of the resonant SESAM on the pulse shortening was first studied in the cavity with a round trip time of 13 ns. The lasing wavelength was controlled with intracavity etalon in order to change the effective modulation depth as shown in Figure 5.1. The pulse shortened from 360 ns to 60 ns when changing the modulation depth from 5 % to 40 %. The pulse width was further decreased by shortening the cavity by removing the passive fiber which resulted in a cavity round trip time of 2.5 ns. The pulse duration was decreased, as expected, all the way to 8 ns with 70 % modulation depth.

Figure 5.2 shows the experimental results of the pulse duration dependence on the absorber modulation depth and cavity round trip time. The results of numerical simulation

of the laser dynamics using the model developed in (11), (12) are shown in this figure with a solid curve. It should be mentioned that the excellent agreement between experimental data and calculations has been achieved without adjustable parameters. This indicates that assumptions made in the model, particularly that the saturable absorber is fully saturated and the gain is efficiently depleted, are indeed applicable to the laser. Figure 5.2 also shows that an excessive increase of ΔR beyond 70% does not result in a notable reduction of the pulse width.

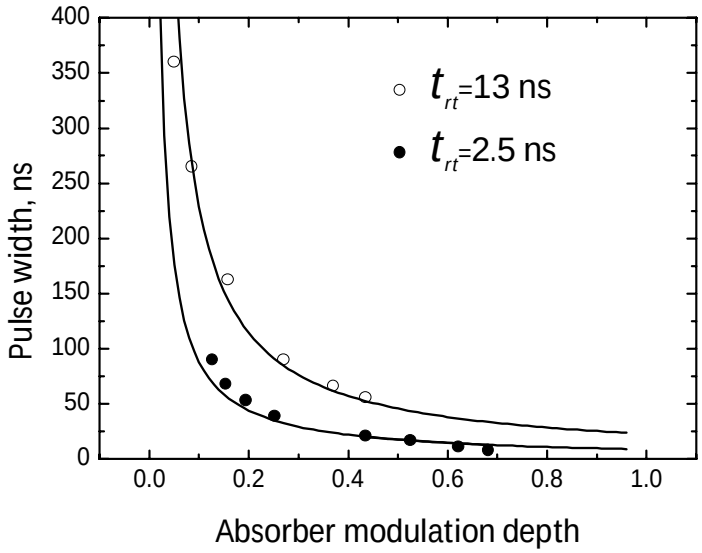

Figure 5.2: Dependence of the pulse duration on the absorber modulation depth and cavity round trip time. Solid curves show the results of numerical modeling which are in excellent agreement with experimental data.

The typical shape of a passively Q-switched pulse was clean without substructure, as seen from the real-time oscilloscope trace in Figure 5.3. The corresponding pulse spectrum is shown as an inset.

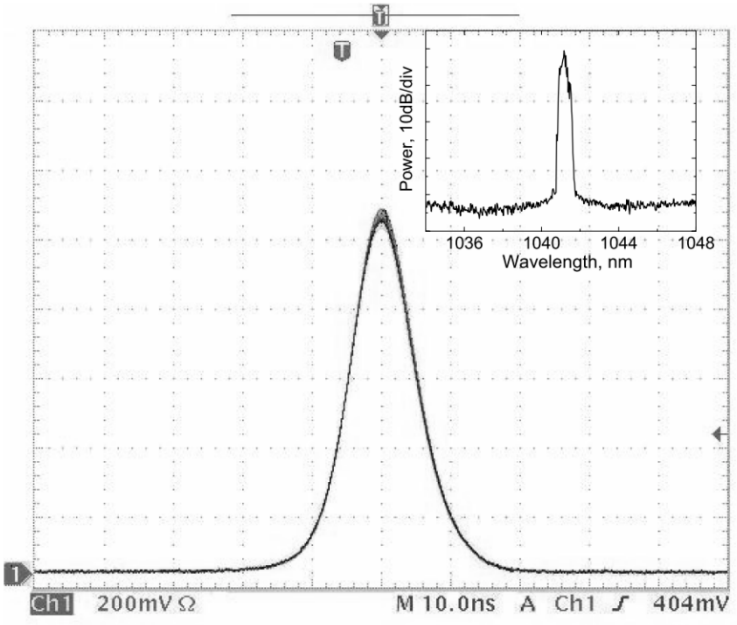

Figure 5.3: Real-time trace from oscilloscope showing ~10 ns Q-switched pulse obtained for the laser cavity with round trip time of 2.5 ns. The x scale is 10 ns per division. The corresponding optical spectrum is shown as an inset.

The resonant SESAMs have proved to be an efficient way to reduce the pulse duration in passively Q-switched fiber lasers. The high modulation depth of a resonant SESAM together with the short cavity length made possible by highly doped gain fiber and an innovative cavity design led to record value in passively Q-switched fiber laser pulse duration.

5.2 Advantages and limitations of Q-switched fiber lasers.

The general advantages of fiber lasers – high gain and good beam quality but long cavity – are certainly applicable to Q-switched fiber lasers, too. Particularly, high gain makes it possible to use saturable absorbers with high modulation depth, which is the key parameter in achieving shorter pulses. On the other hand, fibers have relatively low gain and pump absorption *per unit length* compared e.g. to bulk and microchip solid-state lasers due to limitations in achievable doping levels, which in turn prevents significant reduction in cavity length and consequently limits the potential for pulse width reduction. The pulse energy is typically low for single-mode fiber lasers. However, it could be considerably increased by using double-clad fibers, which accept poor pump beam quality but still retain superb output beam quality. On the other hand, double-clad fibers typically require even longer length since they exhibit lower pump absorption than single mode fibers. However, by using doped photonic crystal fibers as gain media, promising results have been achieved in terms of pulse energy and pulse width: millijoule pulse energies with ~10ns pulse durations have been reported from rod-type Yb-doped photonic crystal fiber (53), (54).

High beam quality at high powers is easier to maintain with fiber lasers compared to bulk solid-state lasers. On the other hand, when very high pulse energies are launched into fiber, thermal lensing, and fiber nonlinearities including self-focusing, the Raman effect and

Brillouin scattering may limit the achievable pulse energy. The nonlinear effects accumulated in a long fiber could be higher than in bulk materials by a few orders of magnitude.

Passively Q-switched fiber lasers may suffer from very high jitter, tens of microseconds. For applications requiring low jitter, actively Q-switched fiber lasers should be primarily considered. Finally, robustness, simplicity and cost-effectiveness represent practical advantages of fiber technology over bulk solid state counterparts.

5.3 Towards higher pulse energies using Master Oscillator Power Amplifier (MOPA)

Q-switched pulses are used in many applications, e.g. in industry, for marking, trimming, and machining. Q-switched pulses can be used also as sources for new wavelengths in the visible and ultraviolet spectrum by frequency conversion. These applications require high pulse energies. It should be considered whether the high pulse energies will be generated by building an oscillator which is already at millijoule level, or by having a low-power oscillator followed by a power amplifier. Both concepts have their good and bad sides, which I'm going to summarize below. While discussing MOPAs, I will concentrate mostly on a special case, the master oscillator fiber amplifier (MOFA).

In principle the amount of complexity is increased when choosing the MOPA approach: the number of pump (diode) lasers as well as other components such as dichroic mirrors, lenses, isolators etc. is increased. Naturally this increases the price and size of the setup, too. Moreover, the wall-plug efficiency of a MOPA is usually worse than that of a laser with corresponding specifications. MOPAs and especially MOFAs are sensitive to back reflections. With a fiber system this is more pronounced due to high gain: the back reflections might get amplified and coupled back to the oscillator and disturb the laser operation or even damage the components. However, using MOPA has certain advantages which may render it very desirable: reaching the final specifications might be a lot easier in terms of wavelength tunability, controlling the pulse repetition rate, pulse width or even pulse shape and beam quality. In general, designing and building a low-power oscillator with desired specifications is easier than a high power one, since generating high power can be decoupled from other design aspects. One can e.g. choose a simple diode laser for the master oscillator and modulate it with desired parameters, as described in (P2). When comparing a MOFA and fiber laser, the intensities are lower in the amplifier fiber than in intracavity gain fiber, which reduces the problems caused by nonlinear effects. However, the nonlinearities are still a bad feature of MOFA, especially at high pulse energies and compared with MOPAs having a bulk gain medium.

Some impressing achievements have been made with nanosecond MOFA amplification in recent years. In 2002, J. Limpert *et al.* reported on the amplification of Q-switched pulses from a Nd:YAG thin-disk laser in a Yb-doped large-mode-area fiber producing an average

power up to 100W. The pulse energies were up to 4 mJ and the repetition rate ranged from 3 to 50 kHz (56). F. Di Teodoro *et al.* reported diffraction-limited 300-kW peak power pulses amplified in 7.0 meters of Yb-doped double-clad fiber using a Q-switched Nd:YAG microchip laser as a pulse source. The pulse width, repetition rate, and pulse energy were 0.8 ns, ~8 kHz, and 255μJ, respectively. Single mode operation was achieved by bend-loss mode filtering. The active fiber was coiled on two cylindrical spools having diameters of 1.67 cm and oriented orthogonally to ensure suppression of both helical polarities of LP_{11} mode (57).

The aforementioned results were realized by cw-pumping. However, Q-switched pulse trains with low, <1 kHz repetition rates have proved to be more challenging for effective amplification. Low repetition rates, even single-shot operation, find applications e.g. in range finding. Continuous wave pumped amplification of low repetition rate pulse trains will cause strong amplified spontaneous emission (ASE) or even spurious lasing (58) between the pulses, which will deplete the upper-state population energy and decrease the amplification efficiency. This can be solved by pulsed pumping, which unavoidably adds some complexity to the system. C. Ye *et al.* reported a pulse-pumped Yb-fiber amplifier which could deliver 138.2 μJ pulses with 0.83 ns duration and 167 kW peak power. The repetition rate could be set freely from single-shot to 1 kHz. This was realized by proper triggering of two drivers for the seed laser and pump diode separately (59). C. Bohling *et al.* also studied pulsed pumping and optimal delay and duration of the amplifier pump pulses. The generated 1.4 mJ and 1.0 ns pulses with 200 Hz repetition rate will result in a huge intensity of 445 GW/cm^2 when focused to a spot of 20 μm in diameter (60).

6. Stabilization of Q-switched operation

A practical pulse source for e.g. industrial applications must have a stable pulse train. The fluctuation in the timing of the pulses in the pulse train is commonly referred to as timing jitter. The timing jitter of a passively Q-switched fiber laser is typically rather large, a few tens of microseconds. This is caused by fluctuations in temperature, pump power, cavity loss, etc., and is recognized as an intrinsic and inevitable feature because the lasing modes start from noise-like spontaneous emission (61). Due to the waveguiding geometry and a relatively long cavity, fiber lasers have a high-level of intracavity spontaneous emission and thus the fluctuations are more pronounced.

In (P4) we studied a method for stabilizing the pulse train of a passively Q-switched ytterbium fiber laser by an optically-driven saturable absorber reflection modulator (SARM), which proved to reduce the timing jitter by a factor of 1.66×10^3 from 50 μs to 30 ns. SARM provided both passive pulse shaping and active locking of the pulse train to a periodic control signal, simultaneously.

The linear fiber cavity of the Q-switched laser studied here is terminated by lens-coupled SARM and a narrow bandwidth fiber Bragg grating (FBG) with a reflectivity of 65% at 1035 nm, as shown in Figure 6.1. The core-pumped 10-cm-long ytterbium doped gain fiber has an absorption of 1348 dB/m at pump wavelength 980 nm. The cavity roundtrip time is 11.6 ns with a focused beam diameter at the modulator of 8.4 μm.

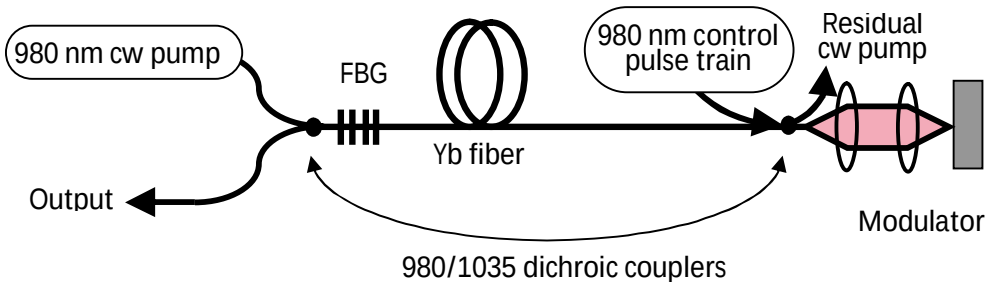

Figure 6.1: Q-switched fiber laser with saturable absorber mirror acting also as a modulator triggered with a control signal. The fiber Bragg grating (FBG) and the modulator define the linear cavity. The fiber coupled pump diodes are protected by free-space isolators. The absorber modulator was protected against residual (non-absorbed in ytterbium fiber) cw 980-nm pump by a second 980/1035-nm dichroic coupler also used for launching 980-nm control signal into the cavity.

The modulator used in this study was fabricated by solid-source molecular-beam epitaxy on n-type GaAs (100) substrate. The sample includes a bottom mirror comprising 30.5 pairs of AlAs/GaAs quarter-wave layers forming a distributed Bragg reflector (DBR) with the center wavelength of 1060 nm and a 100-nm bandwidth. The absorber section comprises 13

InGaAs quantum wells with 6.9-nm thickness. To enhance the modulation response of the SARM, the absorbing quantum wells were placed at the antinodes of the optical standing-wave pattern formed in the microcavity. The modulator is built of a high-quality lattice-matched quantum-well structure to achieve long recovery time of absorption (>1 ns) and thus to reduce possible loss for Q-switched pulse. Due to this, the nonsaturable loss α_{ns} was also very low (≤0.5%). When this is the case, the resonant dip at the wavelength of 1035 nm in the low-intensity reflectivity spectrum shows the achievable modulation depth of 35% defined as the difference between unity and low intensity reflectivity, $\Delta R = 1 - R_{linear} - \alpha_{ns} \approx 1 - R_{linear}$ as shown in Figure 6.2. In addition to the normal use of the absorber mirror, the laser setup allows for optical modulation of the reflection response of the absorption using a control signal.

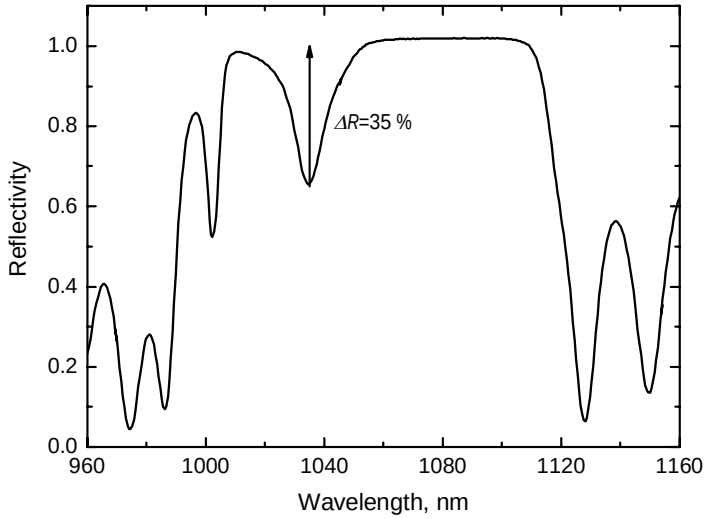

Figure 6.2: Low-intensity reflectivity spectrum of the modulator structure used in this study. Repetitive passive Q-switching was achieved near the 1035 nm resonant wavelength of the monolithic semiconductor microcavity formed by the DBR and Fresnel reflection at semiconductor-air interface.

The Bragg wavelength of the fiber grating was chosen to be centered at 1034.5 nm, corresponding to the resonant wavelength of the semiconductor modulator, and during Q-switched operation it preserved the spectrally narrow-bandwidth performance. In our experiments, the Q-switched single-mode fiber laser was core-pumped with a fiber-coupled, 125 mW, 980-nm diode laser. The optical control signal was generated using another 980-nm diode laser by direct current modulation. The control signal at 980 nm induces a reflectivity change at the lasing wavelength of 1035 nm by partial saturation of the quantum well absorption. The Q-switched pulse then tends to be temporally trapped by the lower-loss absorption window. Figure 6.3 shows the response of the SARM to the modulating 980 nm pulses monitored in the reflection scheme using a low intensity probe signal at 1035 nm. The modulation signal was similar to that used in the locking experiment. At off-states of the modulation the reflectivity of the SARM was found to be 65 % and during the modulation

pulse 81.5 %. The Q-switched pulse, however, dominates the saturation of the absorption leading to a reflectivity of 99.5 % according to nonlinear reflectivity measurements.

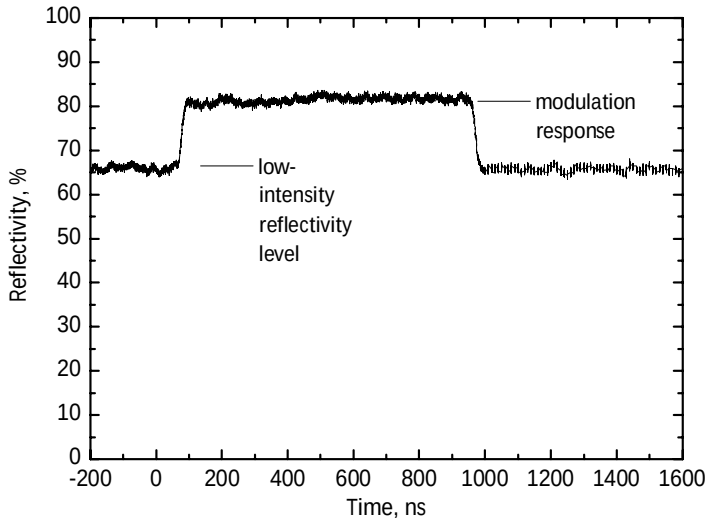

Figure 6.3: The reflectivity change caused by the modulating pulse monitored by a probe signal at 1035 nm. The control signal partially saturates the absorption and causes an increase of the reflectivity during the pulse. The Q-switched pulse locks to the lower-loss window caused by modulation.

The typical average power of the control signal at 5 kHz and 750 ns pulse width was 144 µW. This gives a pulse energy of 28.8 nJ and demonstrates that a low-energy control signal is suitable for synchronization and jitter reduction. The control pulses firmly locked the pulse repetition rate near the frequency of the free-running purely passive Q-switched operation $f_{free\text{-}run}$. With an increase in the modulation frequency f_{mod}, the Q-switched pulse repetition rate f_{rep} first increases accordingly ($f_{rep}=f_{mod}$) until $f_{mod} \leq$ (1.4–1.6)× $f_{free\text{-}run}$. For higher modulation frequencies, the pulse repetition rate switches to a certain subharmonic of the modulation frequency, as seen in Figure 6.4.

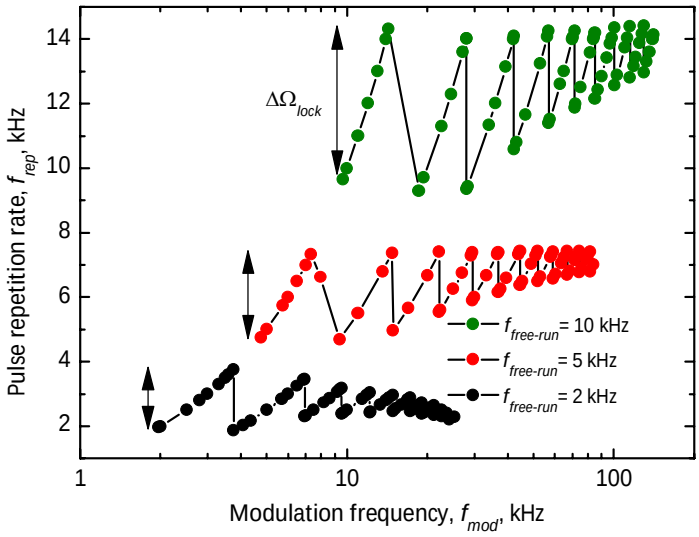

Figure 6.4: Q-switched pulse repetition rate for three different pump powers corresponding to the free-running (non-synchronized) repetition frequencies $f_{free\text{-}run}$ of 2, 5 and 10 kHz. Modulation frequency was ramped up in this experiment starting from $f_{free\text{-}run}$. The locking bandwidth $\Delta\Omega_{lock}$ is indicated by the length of the arrows.

Figure 6.4 shows the frequency locking performance of a Q-switched laser for 3 different pump powers corresponding to $f_{free\text{-}run}$ of 2, 5 and 10 kHz. As can be seen from this plot, with an increase in the modulation frequency f_{mod}, the Q-switched pulse repetition rate f_{rep} first increases accordingly ($f_{rep} = f_{mod}$) until f_{mod} exceeds the value of (1.4–1.6)× $f_{free\text{-}run}$ which denotes the upper level of the locking bandwidth $\Delta\Omega_{lock}$ indicated in Figure 6.4 by the length of the arrows. For higher modulation frequencies, the pulse repetition rate switches to a certain subharmonic M of the modulation frequency, $f_{rep} = f_{mod}/M$. For instance, for the Q-switching regime with $f_{free\text{-}run}$ =5 kHz, the 11th subharmonic at f_{mod} =83 kHz resulted in $f_{rep} = f_{mod}/M \approx 7.55$ kHz=1.5× $f_{free\text{-}run}$.

The pulse-to-pulse timing jitter of the Q-switched fiber laser was measured directly from oscilloscope traces. It can be seen from Figure 6.5(a) that without modulation-induced stabilization, the Q-switched pulse builds up with a large timing jitter of ~50 µs. By contrast, with the control signal activated, timing jitter remained below 30 ns, as shown in Figure 6.5(b). In Figure 6.5(a) the oscilloscope has been triggered on one pulse, and the subsequent pulse has been recorded to a histogram for 2 s. In Figure 6.5(b) the oscilloscope has been triggered to the control pulse, and the timing jitter of the first pulse was recorded with a similar histogram. The technique used in Figure 6.5(a) was not possible in this case, since the jitter was too low to be observed at that scale. This technique proved to reduce the timing jitter in the Q-switched ytterbium fiber laser by more than a factor of 1.66×10^3.

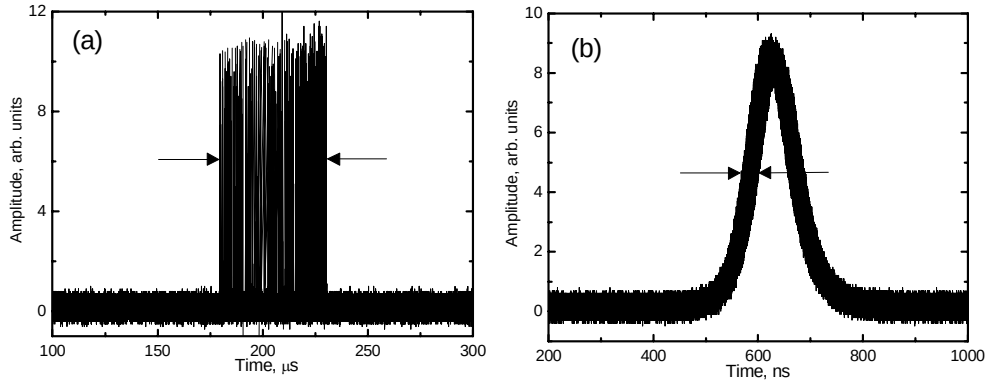

Figure 6.5: Timing jitter shown as a histogram recorded with a digital oscilloscope and a photodiode from laser output for 2 s. With activated control signal, the timing jitter reduces from 50 μs (a), for free-running passive Q-switching down to 30 ns (b). The timing jitter has been defined as shown in the Figure by the arrow gap.

7. Conclusions

This thesis dealt with characterization of semiconductor saturable absorber mirrors (SESAMs) in different operation regimes. Another emphasis was realizing passively Q-switched fiber lasers based on SESAM technology. The main achievements of this study are summarized as follows:

The dependence of the nonlinear response of a SESAM on the temporal characteristics of the incident pulse was studied. The strong dependence of the effective saturation fluence of the saturable absorber on the absorption recovery time of the sample and incident pulse width was proved by empirical experiments and confirmed by modeling. Moreover, a simple method of absorption recovery time determination was developed based on nonlinear reflectivity measurements with different pulse durations.

The temporal response of the SESAM was tuned by the combined action of Ni-ion irradiation and thermal annealing. Ni-ion irradiation shortens the absorption recovery time effectively. It was shown that by use of a proper annealing recipe the absorption recovery time could be tailored from values corresponding to the slow as-grown absorber to those obtained using Ni-ion irradiation. Thermal annealing was shown to decrease the nonsaturable losses and was also expected to have a positive impact on the long-term operation due to the removal of the short-lived states, both caused by irradiation.

The resonant saturable absorber mirrors were used in passive Q-switching of an Yb-fiber laser. The high modulation depth of 70 % combined with a short cavity design resulted in 8 ns pulses, which are to date the shortest realized by passively Q-switched fiber laser.

Passively Q-switched fiber lasers suffer typically from high timing jitter, i.e. pulse-to-pulse timing instabilities. This detrimental effect was reduced by a factor of 1.66×10^3 from 50 µs to 30 ns with an optically driven saturable absorber modulator.

References

1. A. Einstein, *Über einen die Erzeugung und Verwandlung des Lichtes betreffenden heuristischen Gesichtspunkt (On a Heuristic Viewpoint Concerning the Production and Transformation of Light)*, Annalen der Physik, Vol. 17, pp. 132–148, (1905).

2. A. Einstein, *Zur Quantentheorie der Strahlung (On the Quantum Mechanics of Radiation),* Physikalische Zeitschrift, Vol. 18, pp. 121–128, (1917).

3. G. F. Smith, *The early laser years at Hughes Aircraft Company.* IEEE Journal of Quantum Electronics, Vol. 20, 6, pp. 577–584, (1984).

4. T. H. Maiman, *Stimulated optical radiation in ruby*, Nature, Vol. 187, pp. 493–494 (1960).

5. R. N. Hall, G. E. Fenner, J. D. Kingsley, T. J. Soltys, and R. O. Carlson, *Coherent light emission from GaAs junctions.*, Physical review letters, Vol. 9, pp. 366–368, (1962).

6. A. Galvanauskas, C-H. Liu, S. Heinemann, B. Ehlers, A. Carter, K. Tankala, and J. Farroni. *KW-Power Fiber Lasers with Single Transverse Mode Output.* [Online] Nufern, September 22, 2005. [Cited: March 23, 2010.] http://www.nufern.com/whitepaper_detail.php/30.

7. E. Snitzer, *Optical maser action of* Nd^{3+} *in a Barium crown glass.* 12, Physical review letters, Vol. 7, pp. 444–446, (1961).

8. C. J. Koester and E. Snitzer. *Amplification in a Fiber Laser.*, Applied Optics, Vol. 3, 10, pp. 1182–1186, (1964).

9. J. Stone, C. A. Burrus, A. G. Dentai, and B. I. Miller, *Nd:YAG single-crystal fiber laser: Room-temperature cw operation using a single LED as an end pump*, Applied Physics Letters, Vol. 29, 1, pp. 37–39, (1976).

10. A. E. Siegman, *Lasers.* Mill Valley : University Science Books, pp. 1008–1022. (1986).

11. J. J. Zayhowski and P. L. Kelly. *Optimization of Q-switched laser.*, IEEE Journal of Quantum Electronics, Vol. 27, p. 2220, (1991).

12. J. J. Zayhowski and C. Dill III. *Diode-pumped passively Q-switched picosecond microchip lasers.*, Optics letters, Vol. 19, pp. 1427–1429, (1994).

13. J. B, Jhurgin, F. Jin, G. Solyar, C. Wanf, and S. Trivedi, *Cost-effective low timing jitter passively Q-switched diode-pumped solid-state laser with composite pumping pulses*, Applied Optics, Vol. 41, pp. 1095–1097, (2002).

14. B. Cole, L. Goldberg, C. W. Trussell, A. Hays, B. W. Schilling, and C. McIntosh. *Reduction of timing jitter in a Q-Switched Nd:YAG laser by direct bleaching of a Cr^{4+}:YAG saturable absorber*, Optics Express, Vol. 17, pp. 1766–1771, (2009).

15. W. G. Wagner and B. A. Lengyel, *Evolution of the Giant Pulse in a Laser*, Journal of Applied Physics, Vol. 34, p. 2040, (1963).

16. O. Svelto, *Principles of Lasers, 3rd ed.* New York : Plenum, pp. 258–263, (1989).

17. G. J. Spühler, R. Paschotta, R. Fluck, B. Braun, M. Moser, G. Zhang, E. Gini, and U. Keller, *Experimentally confirmed design guidelines for passively Q-switched microchip lasers using semiconductor saturable absorbers*, Journal of the Optical Society of America B, Vol. 16, pp. 376–388, (1999).

18. S. Y. Set, H. Yaguchi, Y. Tanaka, M. Jablonski, Y. Sakakibara, M. Tokumoto, H. Kataura, Y. Achiba, K. Kikuchi, and S. Yamashita, *A Dual-Regime Mode-Locked/Q-Switched Laser using a Saturable Absorber Incorporating Carbon Nanotubes (SAINT).* CLEO'03. Baltimore, MD. Vol. CThPDA9 (2003).

19. A. Szöke, V. Daneu, J. Goldhar, and N. A. Kurnit. *Bistable optical element and its applications.* Applied Physics Letters, Vol. 15, p. 376, (1969).

20. R. Grange, M. Haiml, R. Paschotta, G.J. Spühler, L. Krainer, M. Golling, O. Ostinelli, and U. Keller, *New regime of inverse saturable absorption for self-stabilizing passively mode-locked lasers*, Applied Physics B: Lasers and Optics, Vol. 80, pp. 151–158, (2005).

21. M. Tomita and M. Matsuoka, *Ultrafast pump-probe measurement using intensity correlation of incoherent light.* Journal of the Optical Society of America B, Vol. 3, p. 560, (1986).

22. V. D. S. Dhaka, *Ultrafast Capture and Relaxation of Carriers in InGaAs Semiconductor Quantum-well Nanostructures,* PhD thesis. Vol. 627, Tampere University of Technology, Tampere, (2006).

23. S. Schmitt-Rink, D. Chemla, and D. A. B. Miller, *Theory of transient excitonic optical nonlinearities in semiconductor quantum-well structures,* Physical review B, Vol. 32, pp. 6601–6609, (1985).

24. S. Gupta, J. F. Whitaker, and G. A. Mourou, *Ultrafast Carrier Dynamics in III-V Semiconductors Grown by Molecular-Beam Epitaxy at Very Low Substrate Temperatures.*, IEEE Journal of quantum electronics, Vol. 28, pp. 2464–2472, (1992).

25. R. Takahashi, Y. Kawamura, and H. Iwamura., *Ultrafast 1.55 μm all-optical switching using low-temperature-grown multiple quantum-wells.* Applied Physics Letters, Vol. 68, p. 153–155, (1996).

26. M. Haiml, U. Siegner, F. Morier-Genoud, U. Keller, M. Luysberg, P. Specht, and E.R. Weber, *Femtosecond response times and high optical nonlinearity in beryllium-doped low-temperature frown GaAs,* , Applied Physics Letters, Vol. 74, p. 1269 (1999).

27. A. Marceaux, S. Loualiche, O. Dehaese, and B. Lambert, *High-speed 1.55 μm Fe-doped multiple-quantum-well saturable absober on InP*, Applied Physics Letters, Vol. 78, p. 4065, (2001).

28. M. J. Lederer, B. Luther-Davies, H. H. Tan, and C. Jagadish, *GaAs based antiresonant Fabry-Perot saturable absorber fabricated by metal organic vapor phase epitaxy and ion implantation*, Applied Physics Letters, Vol. 70, p. 3428, (1997).

29. E. L. Delpon, J. L. Oudar, N. Bouché, R. Raj, A. Shen, N. Stelmakh, and J. M. Lourtioz, *Ultrafast excitonic saturable absorption in ion-implanted InGaAs/InAlAs multiple quantum wells,* Applied Physics Letters, Vol. 72, p. 759, (1998).

30. Y. Silberberg, P.W. Smith, D.A.B. Miller, B. Tell, A. C. Gossard, and W. Wiegmann, *Fast nonlinear optical response from proton-bombarded multiple quantum-well structures,* Applied Physics Letters, Vol. 46, p. 701, (1985).

31. J. T. Gopinath, E. R. Thoen, E. M. Koontz, M. E. Grein, L. A Kolodziejski, E. P. Ippen, and J. P. Donnelly, *Recovery dynamics in proton-bombarded semiconductor saturable absorber mirrors*, Applied Physics Letters, Vol. 78, p. 3409, (2001).

32. O. Ostinelli, W. Bächtold, H. Haiml, R. Grange, U. Keller, E. Gini, and G. Almuneau, *Carrier lifetime reduction in 1.5 μm AlGaAsSb saturable absorbers with air and AlAsSb barriers*, Applied Physics Letters, Vol. 89, p. 071114, (2006).

33. S. Suomalainen, A. Vainionpää, O. Tengvall, T. Hakulinen, S. Karirinne, M. Guina, O. G. Okhotnikov, T. G. Euser, and W. L. Los, *Long-wavelength fast semiconductor saturable absorber mirrors using metamorphic growth on GaAs substrates,* Applied Physics Letters, Vol. 87, p. 121106, (2005).

34. S. Suomalainen, M. Guina, T. Hakulinen, O. G. Okhotnikov, T. G. Euser, and S. Marcinkevicius, *1 μm saturable absorber with recovery time reduced by lattice mismatch.* Applied Physics Letters, Vol. 89, p. 071112, (2006).

35. S. Suomalainen, M. Guina, T. Hakulinen, R. Koskinen, J. Paajaste, M. Karjalainen, M. Saarinen, S. Marcinkevicius, and O. G. Okhotnikov, *Semiconductor saturable absorbers with recovery time controlled by lattice mismatch and band-gap engineering,* Materials Science and Engineering B - Solid State Materials Advanced Technology, Vol. 147, p. 156, (2008).

36. S. Suomalainen, *Technology of Fast As-grown Quantum-Well Semiconductor Saturable Absorbers,* Tampere University of Technology, Vol. 736, (2008).

37. R. Herda and O. G. Okhotnikov, *Effect of amplified spontaneous emission and absorber mirror recovery time on the dynamics of the mode-locked fiber lasers,* Applied Physics Letters, Vol. 86, p. 011113, (2005).

38. N. Xiang, M. Guina, A. Vainionpää, J. Lyytikäinen, S. Suomalainen, M. Saarinen, O. G. Okhotnikov, T. Sajavaara, and J. Keinonen, *Broadband semiconductor saturable absorber mirrors in the 1.55-µm wavelength range for pulse generation in fiber lasers,* IEEE Journal of Quantum Electronics, Vols. QE-38, pp. 369–374, (2002).

39. O.G. Okhotnikov, T. Jouhti, J. Konttinen, S. Karirinne, and M. Pessa, *1.5-µm monolithic GaInNAs semiconductor saturable absorber mode locking of an erbium fiber laser,* Optics Letters , Vol. 28, pp. 364–366, (2003).

40. H.A. Haus, *Theory of mode locking with a fast saturable absorber*, Journal of Applied Physics, Vol. 46, pp. 3049–3058, (1975).

41. U. Keller, K. J. Weingarten, F. X. Kärtner, D. Kopf, B. Braum, I. D. Jung, R. Fluck, C. Honninger, N. Matuschek, and J. Aus Der Au, *Semiconductor saturable absorber mirrors (SESAMs) for femtoseconds to nanoseconds pulse generation in solid-state lasers*, IEEE Journal of Selected Topics in Quantum Electronics, Vol. 2, p. 435, (1996)

42. L. R. Brovelli, U. Keller, and T. H. Chiu, *Design and operation of antiresonant Fabry-Perot saturable semiconductor absorbers for mode-locked solid-state lasers*, Vol. 12, pp. 311–322, (1995).

43. E. Garmire, *Criteria for Optical Bistability in a Lossy Saturating Fabry-Perot,*IEEE Journal of Quantum Electronics, Vol. 25. (1989).

44. R. Häring, R. Paschotta, R. Fluck, E. Gini, H. Melchior, and U. Keller, *Passively Q-switched microchip laser at 1.5 µm,* Journal of Optical Society of America B, Vol. 18, pp. 1805–1812, (2001).

45. A. Agnesi, A. Guandalini, G. Reali, J. K. Jabczynski, K. Kopczynski, and Z. Mierczyk, *Diode pumped Nd: YVO4 laser at 1.34 µm Q-switched and mode locked by V3+:YAG saturable absorber,* Optics Communications, Vol. 194, pp. 429–433. (2001).

46. F. X. Kärtner, L. R. Brovelli, D. Kopf, M. Kamp, I. Calasso, and U. Keller, *Control of solid state laser dynamics by semiconductor devices*, Optical Engineering, Vol. 34, pp. 2024–2036, (1995).

47. R. B. Wilcox, D. F. Browning, M. D. Feit, and B. Nyman, *Fiber Amplifiers and Lasers in Yb:silica,* CLEO/QELS '97, (1997).

48. R. Paschotta, R. Häring, E. Gini, H. Melchior, U. Keller, H. L. Offerhaus, and D. J. Richardson, *Passively Q-switched 0.1-mJ fiber laser system at 1.53 µm*, Optics Letter, Vol. 24, pp. 388–390, (1999).

49. S. C. Huang, S. C. Liu, A. Li, K. W. Su, Y. F. Chen, and K. F. Huang, *AlGaInAs quantum-well as a saturable absorber in a diode-pumped passively Q-switched solid-state laser,* Optics Letters, Vol. 32, pp. 1480–1482, (2007).

50. B. Braun, F. X. Kärtner, G. Zhang, M. Moser, and U. Keller, *56-ps passively Q-switched diode-pumped microchip laser,* Optics Letters, Vol. 22, pp. 381–383, (1997).

51. *Millijoule energies, shortest ever pulses, and more*, Nature Photonics, Vol. 2, p. 19, (2008).

52. P. R. Morkel, K. P. Jedrzejewski, E. R. Taylor, and D. N. Payne, *Short-Pulse, High-Power Q-Switched Fiber Laser*, IEEE Photonics Technology Letters, Vol. 4, pp. 545–547, (1992).

53. J. Limpert, N. Deguil-Robin, S. Petit, I. Manek-Hönninger, F. Salin, P. Rigail, C. Hönninger, and E. Mottay. *High power Q-switched Yb-doped photonic crystal fiber laser producing sub-10 ns pulses*, Applied Physics B, Vol. 81, pp. 19–21, (2005).

54. O. Schmidt, J. Rothhardt, F. Röser, S. Linke, T. Schreiber, K. Rademaker, J. Limpert, S. Ermeneux, P. Yvernault, F. Salin, and A. Tünnermann, *Millijoule pulse energy Q-switched short-length fiber laser,* Optics Letters, Vol. 32, pp. 1551–1553, (2007).

55. L. Orsila, R. Herda, and O.G. Okhotnikov, *Monolithic Fiber Mirror and Photonic Crystal Technology for High Repetition Rate All-Fiber Soliton Lasers,*IEEE Photonics Technology Letters, Vol. 19, pp. 2009–2011, (2007).

56. J. Limpert, S. Höfer, A. Liem, H. Zellmer, A. Tünnerman, S. Knoke, and H. Voelckel, *100-W average-power, high-energy nanosecond fiber amplifier*, Applied Physics B, Vol. 75, pp. 477-479, (2002).

57. F. Di Teodoro, J. P. Koplow, S. W. Moore, and D. A. V. Kliner, *Diffraction-limited, 300-kW peak-power pulses from a coiled multimode fiber amplifier,* Optics Letters, Vol. 27, pp. 518-520, (2002).

58. C. C. Renaud, H. L. Offerhaus, J. A. Alvarez-Chavez, J. Nilsson, W. A. Clarkson, P. W. Turner, D. J. Richardson, and A. B. Grudinin, *Characteristics of Q-Switched Cladding-Pumped Ytterbium-Doped Fiber Lasers with Different High-Energy Fiber Designs,* IEEE Journal of Quantum Electronics, Vol. 37, pp. 199–206, (2001).

59. Changgeng Ye, Ping Yan, Mali Gong, and Ming Lei, *Pulsed pumped Yb-doped fiber amplifier at low repetition rate*, Chinese optics letters, Vol. 3, pp. 249–250, (2005).

60. C. Bohling, H. Zimmermann, K. Hohmann, W. Schippers, and W. Schade, *Synchronised Pulsed Pumped Fiber Amplifiers,* Conference on Lasers and Electro-Optics (CLEO), Baltimore, Maryland, (2007).

61. Jacob B. Khurgin, Feng Jin, Gregory Solyar, Chen-Chia Wang, and Sudhir Trivedi, *Cost-effective low timing jitter passively Q-switched diode-pumped solid-state laser with composite pumping pulses*, Applied Optics, pp. 1095–1097, (2002).

Appendices

Publication 1

T. Hakulinen, R. Herda, and O. G. Okhotnikov, “Nonlinear Response of Saturable Absorber Mirrors for Different Operation Regimes,” *IEEE Photonics Technology Letters,* Vol. 19, No. 5, pp. 333–335 (2007).

Publication 2

T. Hakulinen, R. Herda, and O. G. Okhotnikov, “Effect of post-epitaxial-growth processing on the nonlinear response of saturable absorber,” *Applied Optics*, Vol. 47, No. 9, pp. 1235–1238 (2008).

Effect of post-epitaxial-growth processing on the nonlinear response of saturable absorber

Tommi Hakulinen,* Robert Herda, and Oleg G. Okhotnikov

Optoelectronics Research Centre, Tampere University of Technology, P.O. Box 692, FIN-33101 Tampere, Finland

*Corresponding author: tommi.hakulinen@tut.fi

Received 4 October 2007; revised 22 January 2008; accepted 29 January 2008;
posted 1 February 2008 (Doc. ID 88271); published 18 March 2008

The nonlinear response of an ion-irradiated saturable Bragg reflector, further modified by thermal annealing, has been studied. We demonstrate that the absorption recovery time and the effective saturation fluence dependent on the pulse duration can be tailored over a wide range after epitaxial growth by the proper combination of ion irradiation and subsequent annealing. Thermal treatment is also an efficient means for the reduction of the unbleachable losses and the stabilization of the absorber parameters.

OCIS codes: 140.3510, 140.3538, 160.6000, 190.5970, 230.5590, 320.5540.

1. Introduction

Postgrowth thermal annealing is an important stage in the fabrication of reliable semiconductor saturable absorber mirrors (SAMs) for pulsed lasers, which could offer degradation-free operation [1]. It should be noted that absorbers may be operated with a high density of light intensity and, consequently, may acquire a significant thermal load. Fluences over $1\,\mathrm{J/cm^2}$ are possible even with low average power Q-switched lasers [2]. Therefore, lasers may operate close to the optical damage threshold of $3 \pm 1\,\mathrm{J/cm^2}$ typical for GaAs-based reflectors [3]. The effect of thermal annealing on improving the temporal stability of SAM parameters is based on the removal of short-lived defects. This could, however, also change the absorption recovery time. There is still a need for systematic studies of the thermal postgrowth treatment, which could provide practical guidelines for engineering the SAM response and stability. In this paper we demonstrate that thermal annealing is an effective means for tuning the absorption recovery time of ion-irradiated SAMs and significantly reducing the nonbleachable losses. These factors could have a remarkable impact on the starting capability of pulsed operation and are important for achieving reliable long-term operation.

2. Experimental Details

The absorber section of the SAM comprises three $In_{0.24}Ga_{0.76}AsIn_{0.30}Ga_{0.70}AsIn_{0.24}Ga_{0.76}As$ quantum wells separated by 20 nm thick barriers. The structure is grown monolithically by molecular beam epitaxy on a highly reflective distributed Bragg reflector, which comprises 30.5 pairs of $\lambda/4$ AlAs/GaAs layers. On the top of the absorber 60 nm of GaAs was grown as a cap layer. Irradiation with 6 MeV Ni ions with a dose of $5 \times 10^{11}\,\mathrm{cm^{-2}}$ was applied to reduce the recovery time of absorption to the picosecond level [4]. Annealing of the irradiated samples was performed in a dry nitrogen atmosphere with a protective SiO_2 film deposited by plasma enhanced chemical vapor deposition on the sample prior to annealing to prevent outdiffusion. The ramp-up rate from room temperature to the annealing temperature was 5.5 °C/s. The protective film was etched away after thermal treatment.

The nonlinear response of the structures was derived from the dependence of their reflectivity on the incident pulse fluence. The modulation depth ΔR, saturation fluence F_{sat}, and unbleachable loss α_0 were determined from these measurements. The nonlinear response of the samples was studied using

0003-6935/08/091235-04$15.00/0

a mode-locked fiber laser and a Q-switched fiber laser producing 2 ps and 370 ns pulses, respectively. Both lasers were operating at 1038 nm. The output of the oscillators was amplified in a Yb-doped fiber amplifier. The pulse fluence was set by a variable 30 dB attenuator. The output was split into two beams that provided both the probe and the reference beams. The beam was focused on the absorber using a microscope objective. We measured a beam diameter of 3.1 μm using the knife-edge technique. The intensity of the beams was detected by a dual-channel power meter. The average reflectivity of the SAM was determined as the ratio between the reflected beam and the reference beam. The performance of the absorbers was finally examined by using them in a Yb-doped fiber laser.

3. Results

Figure 1 summarizes the nonlinear reflectivity change for an as-grown slow sample and for ion-irradiated fast absorbers before and after thermal annealing. An absorber with high modulation depth ΔR is typically required to ensure reliable start-up of mode-locking in a fiber laser. It has been shown recently that using a resonant-type absorber allows a large value of ΔR to be achieved while preventing Q-switched instability [5]. The resonant SAM used here has a modulation depth of ~14%. The absorption recovery time τ_a was determined by the method described in [6]. The measurements were performed using both picosecond and nanosecond pulses. The annealing details and the absorption recovery time for as-grown and annealed SAM are listed in Table 1. The effect of thermal annealing on the operation regime can be qualitatively understood using expressions derived from rate equation analysis. Steady-state mode-locking is stable against Q-switched mode-locking if

$$F_P(\mathrm{d}q/\mathrm{d}F_P) < T_r/\tau_L, \tag{1}$$

where F_P is the pulse fluence, q is the saturable absorption, T_r is the cavity round trip times and τ_L is the gain material recovery time [7]. In the continuous wave (cw) mode-locking regime the absorber is strongly saturated. When the pulse duration τ_p is much shorter than the absorption recovery time τ_a, the absorption q saturated by the pulse is given by $q = \Delta R \exp(-F_P/F_{\mathrm{sat},\tau\to 0})$, where $F_{\mathrm{sat},\tau\to 0}$ is the saturation fluence for pulses with $\tau_p \ll \tau_a$. Therefore, the stability against Q-switched mode-locking does not change significantly with an annealed absorber as long as the pulse duration is much shorter than the absorption recovery time and the modulation depth does not vary significantly. In contrast, the stability criterion against Q-switching of the cw-running laser is determined by

$$-2I(\mathrm{d}q/\mathrm{d}I) < T_r/\tau_L, \tag{2}$$

where I is the intracavity intensity [8]. The saturable absorption here is given by $q = \Delta R/(1 + I/I_{\mathrm{sat}})$, where I_{sat} is the saturation intensity. Because the saturation intensity $I_{\mathrm{sat}} = F_{\mathrm{sat},\tau\to 0}/\tau_a$ is inversely proportional to the recovery time and the saturable absorber is weakly saturated for the cw regime, a longer recovery time causes a higher value of the "driving force" $-2I(\mathrm{d}q/\mathrm{d}I)$ and may, therefore, violate the above inequality in Eq. (2) and provoke Q-switched operation. This effect can clearly be seen from Table 1. For lasers with low saturation fluence, the short recovery time and the high modulation depth ensure stable cw mode-locking according to Eq. (1). When the recovery time increases too much (higher than ~100 ps), the value of the driving force for Q-switched operation is high, and the laser remains in Q-switched operation.

The first important observation derived from the measurements is that the modulation depth of the absorber mirror (~14%) is fairly independent of the absorption recovery time, ion irradiation, and regime of thermal annealing. Therefore, high modulation depth absorber mirrors can be treated thermally without detrimental effects on their performance.

Pulse fluences larger than 1 J/cm^2 were not available for these experiments, thus the samples with fast absorption recovery could not be fully saturated with long pulses, as in Fig. 1. The nonlinear response and corresponding effective saturation fluence under these conditions were determined assuming a shape of a plot similar to that observed with picosecond pulses (short pulse response, Fig. 1). The validity of this assumption becomes evident from the comparison of different plots shown in Fig. 1. Here we used the effective saturation fluence $F_{\mathrm{sat,eff}}$ dependent on the incident pulse width, which has been defined in [6], contrary to the conventional definition

Table 1. Effect of Annealing on Absorption Recovery Time and the Regime of Laser Operation

Annealing Parameters	Recovery Time (ps)	Laser operation ML, mode-locking; QS, Q-switching
As-irradiated	2	ML self-starting is critical
400 °C, 30 s	9	Excellent, robust starting of ML
400 °C, 60 s	11	Good starting of ML
400 °C, 120 s	15	ML starting is difficult, double pulsing
600 °C, 30 s	119	QS with some instability
As-grown	170	Stable QS

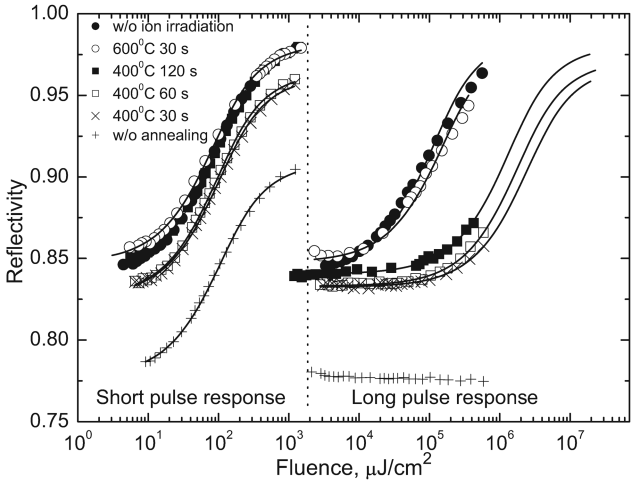

Fig. 1. Change in the reflectivity response of the absorber mirror measured as a function of pulse fluence. Probe pulses measuring 2 ps and 370 ns long have been used to examine an as-grown slow absorber and an irradiated fast saturable absorber before and after annealing.

for saturation fluence that is determined for probe pulses much shorter than the recovery time of absorption [9]. The expected increase in the effective saturation fluence for nanosecond Q-switched pulses compared with picosecond mode-locked pulses can be clearly seen in Fig. 1 by comparing the short and long pulse responses.

Another conclusion that can be derived from Fig. 1 is that with appropriate thermal annealing (600 °C, 30 s), the effect of ion irradiation can be largely eliminated and the parameters of the absorber can be restored, resulting in values typical for an as-grown slow sample observed prior to ion irradiation. Annealing therefore allows the recovery time and, consequently, the effective saturation fluence of the absorption to be set at any value ranging from the characteristic values for fast (after ion irradiation) and slow (as-grown) absorber mirrors.

The plots in Fig. 1 clearly illustrate that it becomes progressively more difficult to saturate the absorber as the recovery time τ_a decreases. In particular, the ion-irradiated fast absorber without thermal annealing shows no sign of saturation with pulses longer than 100 ns. This behavior is more pronounced with a further increase in the pulse duration. Figure 2 plots (filled circles) effective saturation fluence determined from the measurements with a Q-switched laser source as a function of the absorption recovery time. This illustrates the increase in effective saturation fluence with an increase in the speed of the absorption recovery. Another essential though expected feature is a 7% decrease in unbleachable losses with thermal annealing, which is illustrated in the same plot (with empty circles) as a function of absorption recovery time.

The experimental results presented above were further analyzed by modeling the saturable absorber. The saturable losses $q(t)$ of the SAM are described by a rate equation in the form

$$\frac{\mathrm{d}q(t)}{\mathrm{d}t} = -\frac{q(t)-q_0}{\tau_a} - \frac{q(t)I(t)}{F_{\mathrm{sat},\tau\to 0}}, \tag{3}$$

where t is the time, $I(t)$ is the incident intensity, q_0 is the modulation depth, τ_a is the absorber recovery time, and $F_{\mathrm{sat},\tau\to 0}$ is the saturation fluence for pulses much shorter than the absorber recovery time [9]. To examine the absorber response, Eq. (3) was numerically solved for pulses with different durations and different energies. Figure 2 shows the simulated data (half-filled circles) for the effective saturation fluence obtained. Figure 2 also shows a fit (solid curve) using the expression $F_{\mathrm{sat,eff}}/F_{\mathrm{sat},\tau\to 0} = 0.94\tau_{\mathrm{pulse}}/\tau_a$ with $\tau_{\mathrm{pulse}} = 370$ ns [6]. The modeling confirms that the effective saturation fluence is inversely proportional to the recovery time.

Figures 3(a)–3(c) show the simulation results for absorbers with recovery times of 2, 15, and 170 ps, respectively. The contour plots in Fig. 3 show the average saturable losses acquired by the pulse after passing through the absorber. The graphs clearly illustrate that the incident pulse energy required for saturating the absorber increases significantly with a pulse duration larger than the absorber recovery time. It can also be seen from a comparison of Figs. 3(a) and 3(b) that it would be easier to saturate a slow absorber than a fast absorber with Q-switched pulses.

Testing the absorber samples in a fiber laser allowed the observation of all regimes of pulsed operation with the same semiconductor structure, depending on the postgrowth processes applied. This verifies that the parameters of the absorber mirror can be largely tailored by ion irradiation followed by thermal annealing. The Yb fiber laser with a

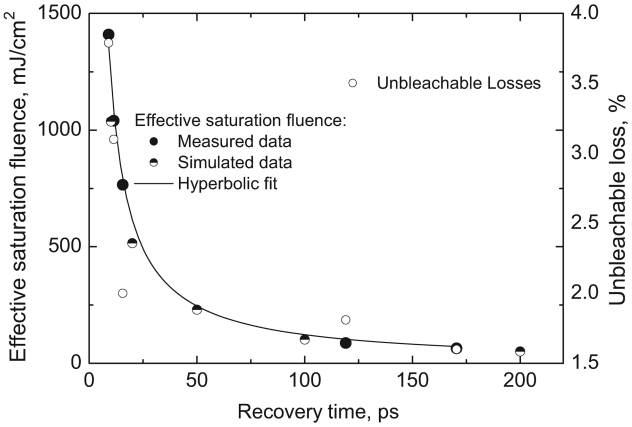

Fig. 2. Unbleachable losses (empty circles) and effective saturation fluence versus recovery time of absorption measured with Q-switched pulses. Measured data (filled circles), simulated data (half-filled circles), and a hyperbolic fit of the measured data are in good agreement, confirming the validity of the absorber model for the effective saturation fluence.

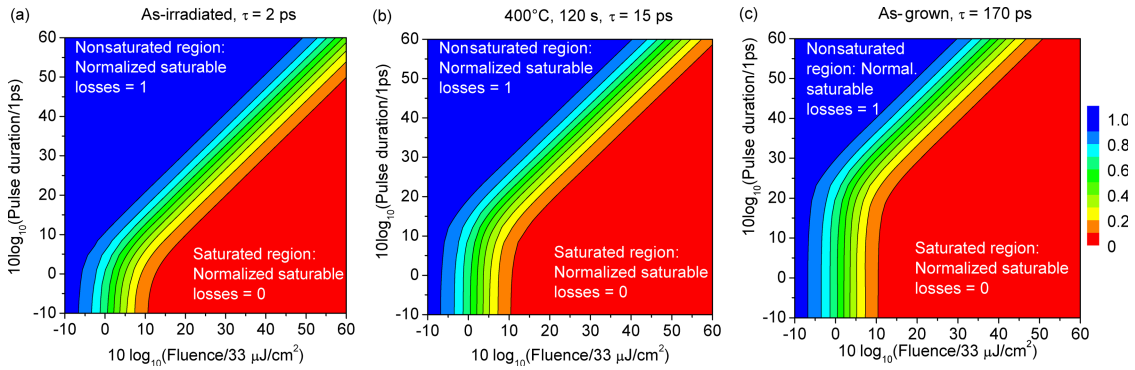

Fig. 3. (Color online) (a)–(c) Saturable losses of a SAM (normalized to the modulation depth) as a function of the fluence and the duration of the incident pulses.

linear cavity terminated by the SAM and an 80% end reflector acting as an output coupler was a test bed for absorber examination. The fiber section of the cavity and the grating pair dispersion compensator provide a round trip cavity anomalous dispersion of $-1\,\mathrm{ps}^2$, which supports the soliton pulse regime in mode-locked operation. Use of this dispersion regime was found to facilitate reproducible replacement of the SAM samples in the cavity and ensure self-starting short pulse operation for an extended range of absorption recovery times compared with the normal dispersion regime. When the pulse formation occurs in a laser with a fast saturable absorber, initially long pulses ($\tau_p \gg \tau_a$) experience a very large effective saturation fluence $F_{\mathrm{sat,eff}}$ and, therefore, propagate in a high-loss regime. This explains why the starting capability of a fast absorber is poor compared to a slow absorber having a low value of $F_{\mathrm{sat,eff}}$ for relatively long pulses. With a gradual increase in absorber recovery time, the effective saturation fluence of the absorption decreases, and eventually approaches the value typical for slow absorbers ($\tau_p < \tau_a$). The fast absorber with short recovery time τ_a is, however, more suitable for shaping short mode-locked pulses because it is efficient in the rejection of the long pulses that suffer large saturation fluence. Therefore, the fast absorber is preferable for selecting the mode-locking regime as compared with the slow absorber where saturation fluence has a weak dependence on pulse duration.

The results show that there is an optimum value for the recovery time of an absorber ($\tau_a \sim 9\,\mathrm{ps}$) that offers both reliable start-up of passive mode-locking and efficient pulse shaping in fiber lasers in excellent agreement with the numerical modeling [10]. Table 1, discussed above, summarizes the effect of annealing on the absorption recovery time and laser operation.

4. Conclusions

In conclusion, we have studied the nonlinear response of a semiconductor SAM as a function of postgrowth processing. We show that the absorption parameters of ion-irradiated absorbers can be optimized by thermal annealing to support the desired operation regime. In addition to causing a decrease in the nonbleachable losses, thermal treatment is expected to have a positive impact on the long-term operation due to the removal of the short-lived states induced by ion irradiation. Using the combined action of ion irradiation and annealing, saturable absorber parameters may be tailored from values corresponding to the slow as-grown absorber to those obtained using high-energy heavy ion irradiation. Different operation regimes of a pulsed laser could thus be achieved with the same semiconductor structure depending on the regime of the postgrowth processing.

References

1. M. J. Lederer, B. Luther-Davies, H. H. Tan, and C. Jagadish, "GaAs based anti-resonant Fabry–Perot saturable absorber fabricated by metal organic vapor phase epitaxy and ion implantation," Appl. Phys. Lett. **70**, 3428–3430 (1997).
2. T. Hakulinen and O. G. Okhotnikov, "8 ns fiber laser *Q* switched by the resonant saturable absorber mirror," Opt. Lett. **32**, 2677–2679 (2007).
3. L. P. Gonzalez, S. Guha, and S. Trivedi, "Damage thresholds and nonlinear optical performance of GaP," *CLEO*, in *Proceedings of IEEE Conference Lasers and Electro-Optics (CLEO)* (IEEE, 2004), paper CWA47.
4. E. Lugagne Delpon, J. L. Oudar, N. Bouché, R. Raj, A. Shen, N. Stelmakh, and J. M. Lourtioz, "Ultrafast excitonic saturable absorption in ion-implanted InGaAs/InAlAs multiple quantum wells," Appl. Phys. Lett. **72**, 759–761 (1998).
5. R. Herda and O. G. Okhotnikov, "Dispersion compensation-free fiber laser mode-locked and stabilized by high-contrast saturable absorber mirror," IEEE J. Quantum Electron. **40**, 893–899 (2004).
6. T. Hakulinen, R. Herda, and O. G. Okhotnikov, "Nonlinear response of saturable absorber mirrors for different operation regimes," IEEE Photon. Technol. Lett. **19**, 333–335 (2007).
7. C. Hönninger, R. Paschotta, F. Morier-Genoud, M. Moser, and U. Keller, "*Q*-switching stability limits of continuous-wave passive mode locking," J. Opt. Soc. Am. B **16**, 46–56 (1999).
8. F. X. Kärtner, L. R. Brovelli, D. Kopf, M. Kamp, I. Calasso, and U. Keller, "Control of solid-state laser dynamics by semiconductor devices," Opt. Eng. **34**, 2024–2036 (1995).
9. H. A. Haus, "Theory of mode locking with a fast saturable absorber," J. Appl. Phys. **46**, 3049–3058 (1975).
10. R. Herda and O. G. Okhotnikov, "Effect of amplified spontaneous emission and absorber mirror recovery time on the dynamics of the mode-locked fiber lasers," Appl. Phys. Lett. **86**, 011113 (2005).

Publication 3

T. Hakulinen and O. G. Okhotnikov, “8 ns fiber laser Q switched by the resonant saturable absorber mirror,” *Optics Letters*, Vol. 32, No. 18, pp. 2677–2679 (2007).

8 ns fiber laser *Q* switched by the resonant saturable absorber mirror

Tommi Hakulinen* and Oleg G. Okhotnikov

Optoelecronics Research Centre, Tampere University of Technology, P. O. Box 692, FIN-33101, Tampere, Finland
**Corresponding author: tommi.hakulinen@tut.fi*

Received June 12, 2007; revised July 31, 2007; accepted August 3, 2007;
posted August 8, 2007 (Doc. ID 84088); published September 4, 2007

We demonstrate that resonant high-modulation-depth saturable absorbers allow efficient pulse shortening in *Q*-switched lasers. Using a 70% modulation depth resonant saturable absorber mirror we achieved 8 ns pulses that are close to the limit set by the cavity length and are, to our knowledge, the shortest pulses demonstrated to date from passively *Q*-switched fiber lasers. © 2007 Optical Society of America

OCIS codes: 060.2320, 140.3480, 140.3510, 140.3540, 140.3600.

Different applications benefit from short high-peak-power pulses. High peak powers can usually be produced by *Q*-switched lasers; however, fiber lasers—one of the most promising type of laser—typically fail to generate pulses shorter than a few hundred nanoseconds because of the relatively long cavity. Passive *Q* switching using semiconductor saturable absorbers has many advantages since the absorber parameters that determine the pulse duration can be tailored in a wide range, particularly, the absorption recovery time and the modulation depth. It has been shown, however, that the decrease in the recovery time of the absorption does not contribute notably to the pulse shortening [1,2], whereas fast saturable absorbers may cause additional losses for long *Q*-switched pulses when the pulse width is notably longer than the recovery time of the absorber ($\tau_{\text{pulse}} \gg \tau_{\text{absorption}}$). Therefore, the modulation depth of the saturable absorber is an exceptional factor in achieving the short pulse regime.

Recently, we have shown that a resonant semiconductor saturable absorber mirror (SESAM) with a high reflectivity change allows reliable start-up of passive mode locking in a wide range of normal or anomalous cavity dispersion and efficiently suppresses the detrimental effect of amplified spontaneous emission [3,4]. Resonant saturable absorbers offer a modulation depth of up to $\Delta R = 100\%$ with a so-called impedance-matched design [5]. This type of SESAM, however, unavoidably induces certain bandwidth restrictions that limit achievable pulse shortening in the mode-locked regime. Therefore, the combination of ΔR and $\Delta\lambda$ is always subject to trade-off in ultrashort pulse lasers. Contrary to mode-locked systems, a narrow-line optical spectrum is typically desired for *Q*-switched lasers. This gives a strong motivation for using high modulation depth resonant-type absorber mirrors in passively *Q*-switched lasers to achieve efficient pulse shortening.

Since the pulse width τ_{pulse} is proportional to the cavity round-trip time τ_{rt} [1], the pulse shortening in a *Q*-switched fiber laser is primarily limited by the cavity length, which cannot be made as short as in other laser types, e.g., microchip lasers. Therefore, increasing the modulation depth ΔR of the absorber mirror is an exceptional opportunity for producing short pulses in *Q*-switched fiber lasers. In this Letter, we propose a resonant saturable absorber for decreasing the pulse duration because it allows significant increase in modulation depth compared with antiresonant Fabry–Perot structures [6]. The large modulation depth can be achieved in an antiresonant geometry only with substantial absorption, e.g., by increasing the number of quantum wells, which in turn unavoidably leads to vast saturation fluence. With resonant configuration, cavity enhanced modulation depth is accompanied by a corresponding reduction in the saturation fluence.

8 ns pulses have been obtained using a resonant absorber with a modulation depth of 70%; to our knowledge, these are the shortest pulses reported to date from passively *Q*-switched fiber lasers. It should be noted that the shortest width of *Q*-switched pulse that could be achieved with an ideal absorber is a few times larger than the cavity round-trip time [1,2,6]. Therefore, reports on the operation of *Q*-switched laser with pulses shorter than the round-trip time, e.g., [7], are likely to originate from temporal instability due to *Q*-switched mode locking when one mode-locked pulse accidentally appears within the *Q*-switched envelope. This operation mode is unlikely to offer long-term stability and cannot be recognized as a pure *Q*-switched operation.

The fiber laser cavity is formed between the lens coupled SESAM and a polished fiber connector, which has a dichroic coating with reflectivity of 65% at 1050 nm and is highly transparent at the pump wavelength. The 15 cm Yb-doped gain fiber, having absorption of 2000 dB/m at 980 nm, was core pumped at 974 nm through the coated connector by a laser diode. The maximum absorbed pump power was 125 mW. A thin Fabry–Perot etalon was placed into the free-space section of the cavity to control the oscillation wavelength. Throughout the experiments, a short piece of passive single-mode (Flexcore 1060) fiber could be spliced to the gain fiber to study the effect of cavity length on the *Q*-switched pulse duration. The cavity round-trip time was first set to 13 ns and then decreased to 2.5 ns by removing the passive (undoped) fiber from the laser cavity. The laser was

0146-9592/07/182677-3/$15.00

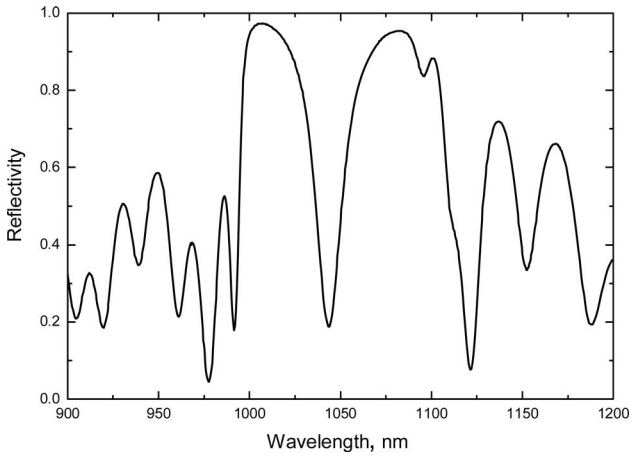

Fig. 1. Low-intensity reflectivity of the resonant semiconductor saturable absorber mirror. The resonant wavelength of the SESAM microcavity is 1043 nm.

capable of producing 20 mW of average output power at the highest available pump power.

The SESAM used in this study was fabricated by solid-source molecular-beam epitaxy on n-type GaAs(100) substrate. The sample includes a bottom mirror comprising 24 pairs of AlAs/GaAs quarter-wave layers forming a distributed Bragg reflector (DBR). The DBR's stop band had a center wavelength of 1050 nm and a 120 nm bandwidth. The absorber section comprises 14 InGaAs quantum wells with 8 nm thickness. The quantum-well structure is sandwiched between a GaAs buffer layer and a 100 nm GaAs cap layer. The thickness of the buffer layer was adjusted to the resonance condition of the Fabry–Perot microcavity formed by the semiconductor DBR and the top reflector at the semiconductor/air interface. The low-intensity reflectivity spectrum of the SESAM used in this study, shown in Fig. 1, reveals the resonant wavelength of 1043 nm. The absorption recovery time of the SESAM was found to be 300 ps. As has been discussed recently, the saturation fluence F_{sat} depends on the pulse duration τ_{pulse} [8]. The saturation fluence of the absorber mirror for Q-switched pulses was found to decrease from 62 to 5 mJ/cm^2 for pulse durations of 125 and 10 ns, respectively. Data show that saturable absorption is indeed highly oversaturated with the pulse, since the fluence at the SESAM exceeds typically the value of 1 J/cm^2. Particularly, operation at the repetition rate of 58.7 kHz with an intracavity average power of 50 mW results in a pulse energy of 0.86 μJ. The diameter of the mode spot at the SESAM of 6.2 μm thus gives the fluence of 2.85 J/cm^2.

First, the performance of the resonant absorber was studied in a laser cavity with a round-trip time of 13 ns. The duration of the Q-switched pulses as a function of the SESAM modulation depth is given in Fig. 2. The results of numerical simulation of the laser dynamics using the model developed in [1,2] are shown in this figure with a solid curve. We could reduce the pulse width from 360 to 60 ns exclusively by increasing the modulation depth of the saturable absorber achieved using wavelength-dependent characteristics of the resonant structure. It should be mentioned that the excellent agreement between experimental data and calculations has been achieved without adjustable parameters. This indicates that assumptions made in the model, particularly that the saturable absorber is fully saturated and the gain is efficiently depleted, are indeed applicable to the laser. Figure 2 also shows that an excessive increase of ΔR beyond 70% does not result in a notable reduction of the pulse width.

Further decrease in the pulse duration could be achieved only by using a cavity with a shorter length comprising exclusively the Yb-doped gain fiber. The plot in Fig. 2 corresponding to the shorter cavity with $\tau_{\mathrm{round\ trip}}=2.5$ ns reveals an expected decrease in the pulse width. The 8 ns pulse achieved for $\Delta R \sim 70\%$ is the shortest pulse duration reported to date from passively Q-switched fiber lasers. The typical shape of a passively Q-switched pulse was clean without

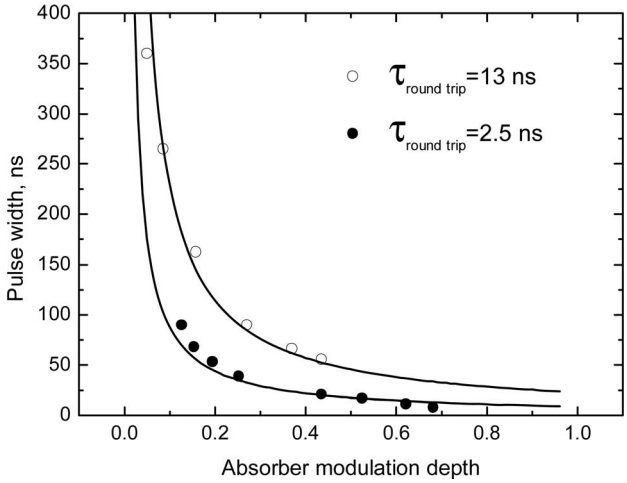

Fig. 2. Duration of the Q-switched pulse depending on the modulation depth of the saturable absorber and cavity length. Solid curves show corresponding results of numerical simulation.

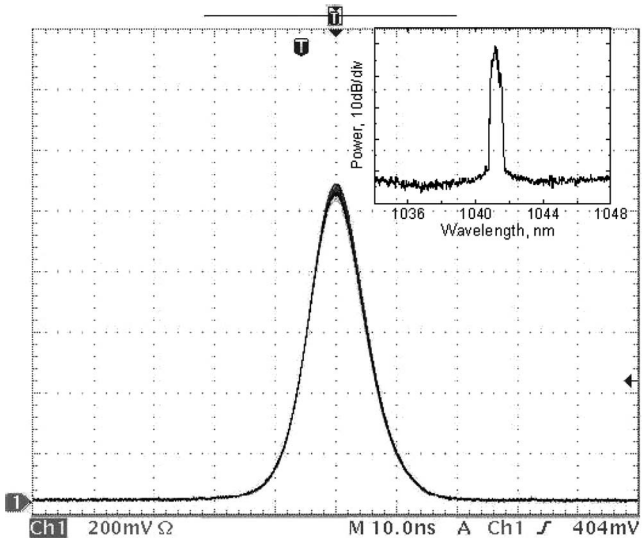

Fig. 3. Real-time trace from oscilloscope showing ~10 ns Q-switched pulse obtained for the laser cavity with round-trip time of 2.5 ns. The x scale is 10 ns per division. The corresponding optical spectrum is shown as an inset.

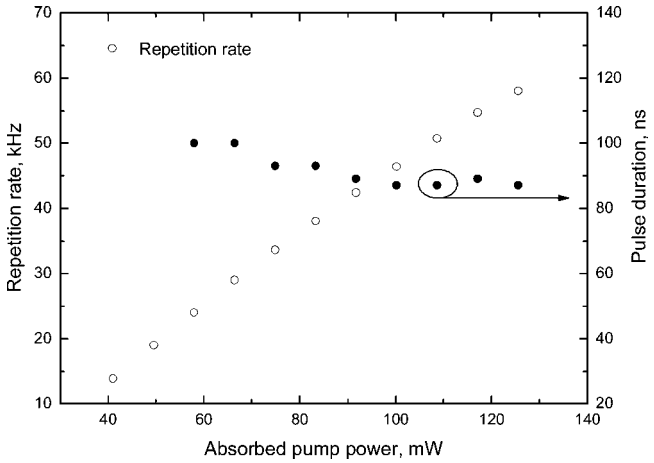

Fig. 4. Pulse width and the repetition rate of the Q-switched Yb-fiber laser as a function of the absorbed pump power. Results were obtained with the laser cavity with a round-trip time of 13 ns.

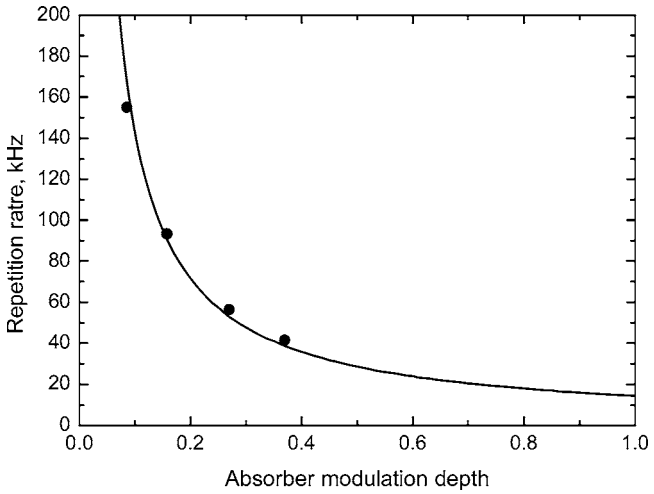

Fig. 5. Repetition rate versus absorber modulation depth corresponding to the measurement presented in Fig. 2 for the laser cavity with round-trip time of 13 ns. The solid curve represents the $f_{\text{repetition}} \sim (\Delta R)^{-1}$ dependence expected from the model.

substructure, as seen from the real-time oscilloscope trace in Fig. 3. The corresponding pulse spectrum is shown as an inset. The typical pulse energy and peak power achieved here with core pumping by one single-mode diode were 0.1 μJ and 10 W, respectively.

The low optical efficiency obtained here is primarily determined by two factors: the low efficiency of the highly doped Yb fiber available for this experiment and the fast recovery of the saturable absorption. An increase in the efficiency and pulse energy is expected with state-of-the-art fiber, particularly, with large mode area fiber [9] and by using high power diodes in a cladding pumping scheme. The increase in the absorption recovery time of the multiple-quantum well semiconductor to 1 ns, and even slightly above would be possible by thorough optimization of the growth conditions [9].

Since the absorber is fully saturated, the pulse duration does not depend noticeably of the pump power, while the repetition rate increases linearly in agreement with the theoretical predictions [2]. This feature is illustrated in Fig. 4 for laser configuration with $\tau_{\text{roundtrip}} = 13$ ns. Because the repetition rate and average output power depend linearly on the pump power, the Q-switched pulse energy was fairly independent of the pump power. For the maximum output power of 20 mW, the repetition rate decreases from 180 to 40 kHz when ΔR increases from 7% to 38%, as shown in Fig. 5. It can be seen from the figure that the data are adequately fitted with $f_{\text{repetition}} \sim (\Delta R)^{-1}$ dependence expected from the model.

In summary, we have found that using resonant saturable absorber mirrors in a Q-switched fiber laser may significantly improve the performance by producing pulses with reduced width. The potential of the resonant saturable absorber has been illustrated through demonstration of pulse shortening in a Q-switched Yb fiber laser by a factor of 7 using a SESAM with a modulation depth of $\Delta R = 45\%$ when compared with an absorber mirror with $\Delta R = 7\%$. The modulation depth of 70% achieved near the resonant wavelength of the absorber microcavity allowed generation of pulses with duration of $\tau_{\text{pulse}} = 8$ ns.

References

1. J. J. Zayhowski and P. L. Kelly, IEEE J. *Q*uantum Electron. **27**, 2220 (1991).
2. J. J. Zayhowski and C. Dill III, Opt. Lett. **19**, 1427 (1994).
3. R. Herda and O. G. Okhotnikov, IEEE J. Quantum Electron. **40**, 893 (2004).
4. R. Herda and O. G. Okhotnikov, Appl. Phys. Lett. **86**, 011113 (2005).
5. E. Garmire, IEEE J. Quantum Electron. **25**, 289 (1989).
6. B. Braun, F. X. Kärtner, G. Zhang, M. Moser, and U. Keller, Opt. Lett. **22**, 381 (1997).
7. M. Laroche, A. M. Chardon, J. Nilsson, D. P. Shepherd, W. A. Clarkson, S. Girard, and R. Moncorgé, Opt. Lett. **27**, 1980 (2002).
8. T. Hakulinen, R. Herda, and O. G. Okhotnikov, IEEE Photon. Technol. Lett. **19**, 333 (2007).
9. R. Paschotta, R. Häring, E. Gini, H. Melchior, U. Keller, H. L. Offerhaus, and D. J. Richardson, Opt. Lett. **24**, 388 (1999).

Publication 4

T. Hakulinen, R. Koskinen, and O. G. Okhotnikov, ”Low jitter Q-switched fiber laser using optically driven surface-normal saturable absorber modulator,” *Optics Express*, Vol. 16, No. 12, pp. 8720–8726, (2008).

Low jitter Q-switched fiber laser using optically driven surface-normal saturable absorber modulator

Tommi Hakulinen*, Riku Koskinen, and Oleg G. Okhotnikov

Optoelectronics Research Centre, Tampere University of Technology,
Korkeakoulunkatu 3, 33720 Tampere
**Corresponding author: tommi.hakulinen@tut.fi*

Abstract: A technique for stabilizing the repetition frequency of a passively Q-switched laser is presented using an optically driven surface-normal semiconductor modulator. A method is capable of significant reduction of the timing jitter in a passively Q-switched laser by optical triggering the saturable absorber semiconductor reflector. The experimental demonstration using passively Q-switched ytterbium-doped fiber laser shows the jitter reduction by factor of 1.66×10^3 from 50 μs down to 30 ns.

OCIS codes: (060.3510) Lasers, fiber; (140.3540) Lasers, Q-switched.

References and links

1. J. J. Zayhowski and C. Dill III, "Diode-pumped passively Q-switched picosecond microchip lasers," Opt. Lett. **19,** 1427–1429 (1994).
2. J. J. Zayhowski and P. L. Kelley, "Optimization of Q-switched Lasers," IEEE J. Quantum Electron. **27,** 2220–2225 (1991).
3. J. J. Degnan, "Optimization of Passively Q-switched Lasers," IEEE J. Quantum Electron. **31,** 1890–1901 (1995).
4. R. Herda, S. Kivistö, and O. G. Okhotnikov, "Dynamic gain induced pulse shortening in Q-switched lasers," Opt. Lett. **33,** 1011–1013 (2008).
5. T. Hakulinen and O. G. Okhotnikov, "8 ns fiber laser Q-switched by the resonant saturable absorber mirror," Opt. Lett. **32,** 2677–2679 (2007).
6. J. B. Khurgin, F. Jin, G. Solyar, C. Wang, and S. Trivedi, "Cost-effective low timing jitter passively Q-switched diode-pumped solid-state laser with composite pumping pulses," Appl. Opt. **41,** 1095–1097 (2002).
7. R. Herda and O. G. Okhotnikov, "Effect of amplified spontaneous emission and absorber mirror recovery time on the dynamics of the mode-locked fiber lasers," Appl. Phys. Lett. **86,** 011113 (2005).

1. Introduction

In different applications of pulsed laser systems, it is necessary to have an accurate control of the temporal characteristics of the pulse train including both the pulse width and the repetition rate. It is known that the duration of the pulses passively Q-switched using saturable absorbers depends critically on the cavity round-trip time, modulation depth of the absorber and the output coupler reflectivity [1-3]. Very recently, a novel mechanism of pulse shortening in a Q-switched laser induced by the gain compression effect under strong pumping conditions has been reported [4]. In passively Q-switched fiber lasers, using high modulation depth saturable absorbers have proved to be an efficient method in short pulse generation. With 70% modulation depth absorber, we have achieved recently a 8-ns pulses, as described in [5]. The modulation depth ΔR of the absorber is determined mainly by the value of the low-intensity reflectivity $R_{L\text{-}I}$ assuming low non-saturable losses ($\alpha_{N\text{-}S}<<1$) in the absorber mirror, $\Delta R=1-R_{L\text{-}I}-\alpha_{N\text{-}S}$. The highest usable modulation depth, therefore, depends largely on the round-trip gain in the cavity, which is essentially high for fiber lasers. Consequently, the usable value of the modulation depth ΔR could be very large particularly for fiber systems

#94703 - $15.00 USD Received 4 Apr 2008; revised 22 May 2008; accepted 26 May 2008; published 29 May 2008

providing convenient means of pulse shortening for passive Q-switched operation. The practical fiber system should, however, in addition offer the high stability of the pulse train repetition rate, whereas the timing jitter of passively Q-switched fiber lasers is rather large, typically of few tens of microseconds. It is well documented that a large timing jitter of a passively Q-switched lasers is caused by fluctuations in temperature, pump, loss, etc, and recognized as an intrinsic and inevitable feature because the "first photon" comes to the lasing mode from noise-like spontaneous emission and imposes a fundamental limit on the stability of the repetition rate [6]. This issue is particularly operative in fiber lasers characterized with a high level of intracavity spontaneous emission owing to the waveguiding geometry and relatively long-length cavity. Intensity of the amplified spontaneous emission captured in a fiber cavity could be comparable with the intensity of the laser emission and, therefore, it can significantly affect the start-up and temporal stability of the pulse regime [7]. In this study we demonstrate a novel method for timing jitter reduction in a passively Q-switched laser using an optically-driven saturable absorber reflection modulator (SARM) that provides both passive pulse shaping and active locking of the pulse train to periodic control signal, simultaneously.

2. Experimental details

The linear fiber cavity of the Q-switched laser studied here is terminated by lens-coupled SARM and a narrow bandwidth fiber Bragg grating (FBG) with reflectivity of 65% at 1035 nm, as shown in Fig. 1. The core-pumped 10-cm-long ytterbium doped gain fiber has absorption of 1348 dB/m at 980 nm. The cavity roundtrip time is 11.6 ns with a focused beam diameter at the modulator of 8.4 μm.

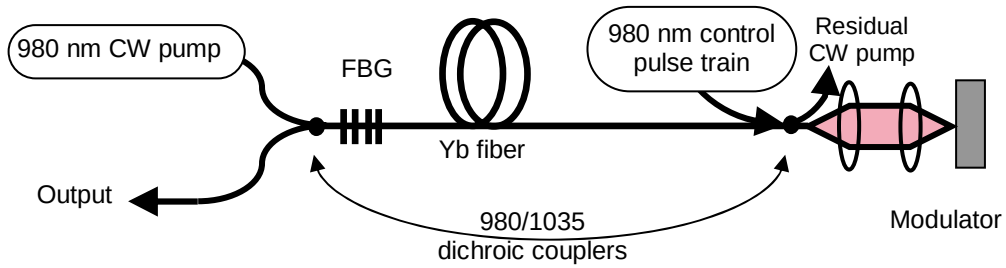

Fig. 1. Q-switched fiber laser with saturable absorber mirror acting also as a modulator triggered with a control signal. Fiber Bragg grating (FBG) and the modulator define the linear cavity. The fiber coupled pump diodes are protected by free-space isolators. The absorber modulator was protected against residual (non-absorbed in ytterbium fiber) CW 980-nm pump by second 980/1035-nm dichroic coupler used for launching into the cavity 980-nm control signal.

The modulator used in this study was fabricated by solid-source molecular-beam epitaxy on *n*-type GaAs (100) substrate. The sample includes a bottom mirror comprising 30.5 pairs of AlAs/GaAs quarter-wave layers forming a distributed Bragg reflector (DBR) with the center wavelength of 1060 nm and a 100-nm bandwidth. The absorber section comprises 13 InGaAs quantum wells with 6.9-nm thickness. To enhance the modulation response of the SARM, the absorbing quantum wells were placed at the antinodes of the optical standing-wave pattern formed in the microcavity. The modulator is built of high-quality lattice-matched quantum-well structure to achieve long recovery time of absorption (>1 ns) and thus to reduce possible loss for Q-switched pulse. Due to this, the non-bleachable loss was also very low (≤0.5%). When this is a case, the resonant dip at the wavelength of 1035 nm in the low-intensity reflectivity spectrum shows the achievable modulation depth of 35% defined as the difference between unity and low intensity reflectivity, as it is defined in the introduction and shown in Fig. 2. In addition to the normal use of the absorber mirror, the laser setup allows for optical modulation of the reflection response of the absorption using a control signal.

#94703 - $15.00 USD Received 4 Apr 2008; revised 22 May 2008; accepted 26 May 2008; published 29 May 2008

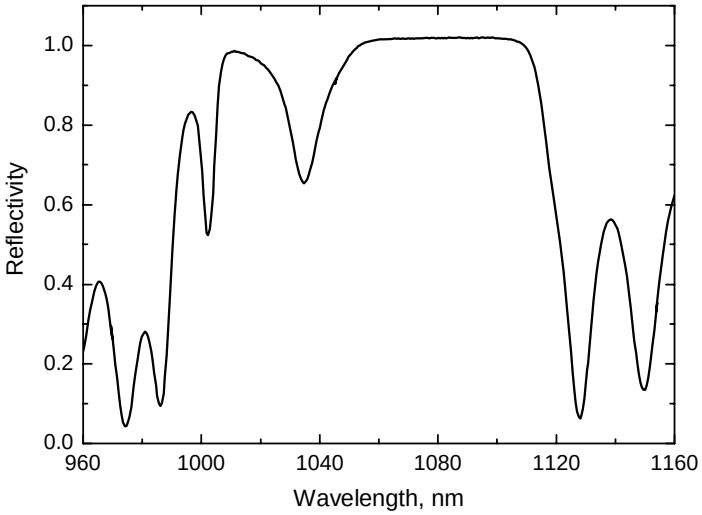

Fig. 2. Low-intensity reflectivity spectrum of the modulator structure used in this study. Repetitive passive Q-switching was achieved near 1035 nm resonant wavelength of the monolithic semiconductor microcavity formed by DBR and Fresnel reflection at semiconductor-air interface.

The Bragg wavelength of fiber grating was chosen to be centered at the 1034.5-nm corresponding to the resonant wavelength of the semiconductor modulator and during Q-switched operation it preserved the spectrally narrow-bandwidth performance. In our experiments, the Q-switched single-mode fiber laser was core-pumped with a fiber-coupled, 125 mW, 980-nm diode laser. The optical control signal was generated using another 980-nm diode laser by direct current modulation. The control signal at 980 nm induces reflectivity change at lasing wavelength of 1035 nm by partial saturation of the quantum well absorption. The Q-switched pulse then tends to be temporally trapped by the lower-loss absorption window. The control pulses locked firmly the pulse repetition rate near the frequency of the free-running purely passive Q-switched operation in a range of $\sim(1\div1.6)\times f_{FREE\text{-}RUN}$, where $f_{FREE\text{-}RUN}$ was determined at a given pump power when the control signal was switched off. Robust locking could be achieved with low-energy modulation. The typical average power of the control signal at 5 kHz and 750 ns pulse width was 144 μW. This gives pulse energy of 28.8 nJ and demonstrates that low-energy control signal is suitable for synchronization and jitter reduction.

Optical modulation response was studied in reflection scheme. Low-intensity cw probe signal at resonance wavelength (1035 nm) and control pulse train at 980 nm were focused on the sample similar to the Q-switched laser setup described in Fig. 1. An additional 75/25-tap coupler was used for monitoring purposes. The reflectivity of the modulator was 65 % at 1035 nm, when modulation was turned off. Modulation response was found from the temporal reflectivity change induced by the control signal, as seen from Fig. 3. The amplitude of the modulation signal was identical to that used in the locking experiment. The modulator reflectivity was found to increase up to 81.5 % at the control pulse time slot. It is, however, obvious that high-energy Q-switched pulse provides the dominant saturation of the absorption resulting in modulator reflectivity of 99.5 %.

#94703 - $15.00 USD Received 4 Apr 2008; revised 22 May 2008; accepted 26 May 2008; published 29 May 2008

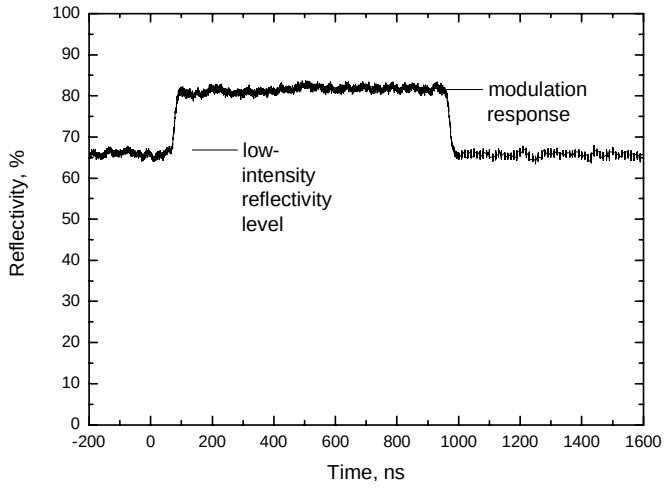

Fig. 3. Modulation response monitored with the probe signal at 1035 nm. Control signal at 980 nm induces a reflectivity change due to partial saturation of the absorption.

3. Results

Figure 4 shows the frequency locking performance of Q-switched laser for 3 different pump powers corresponding to $f_{FREE\text{-}RUN}$ of 2, 5 and 10 kHz. As it can be seen from this plot, with an increase in the modulation frequency f_{MOD}, the Q-switched pulse repetition rate $f_{REPRATE}$ first increases accordingly ($f_{REPRATE}= f_{MOD}$) until f_{MOD} exceeds the value of ~(1.4-1.6)×$f_{FREE\text{-}RUN}$ which denotes the upper level of the locking bandwidth $\Delta\Omega_{lock}$ indicated in Fig. 4 by the length of the arrows. For higher modulation frequencies, the pulse repetition rate switches to the certain subharmonic M of the modulation frequency, $f_{REPRATE}= f_{MOD}/M$. For instance, for the Q-switching regime with $f_{FREE\text{-}RUN}$=5 kHz, the 11th subharmonic at f_{MOD}=83 kHz resulted in $f_{REPRATE}=f_{MOD}/M\approx$7.55 kHz=1.5×$f_{FREE\text{-}RUN}$.

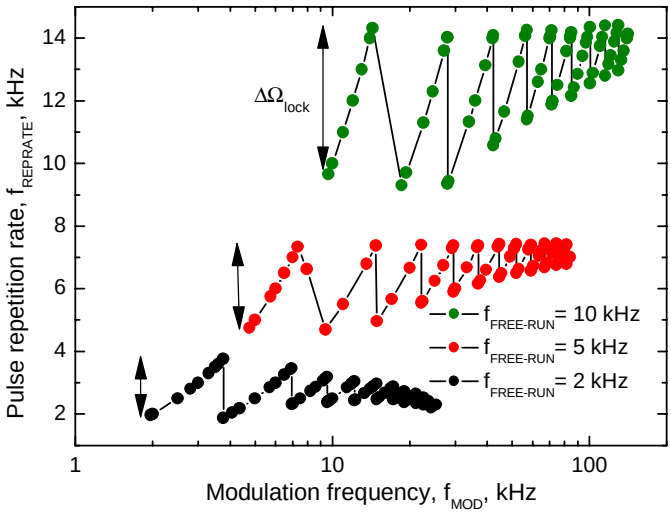

Fig. 4. Q-switched pulse repetition rate for three different pump powers corresponding to the free-running frequencies $f_{FREE\text{-}RUN}$ of 2, 5 and 10 kHz. Modulation frequency was ramping up in this experiment starting from the $f_{FREE\text{-}RUN}$.

#94703 - $15.00 USD Received 4 Apr 2008; revised 22 May 2008; accepted 26 May 2008; published 29 May 2008

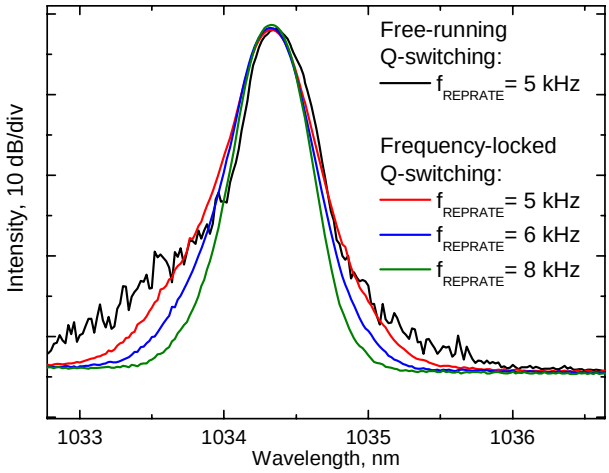

Fig. 5. Optical spectra for identical pump power and different repetition rates set by the control signal.

As it is generally expected, the pump efficiency decreases at low pulse repetition rates in a manner consistent with the spontaneous-relaxation time resulting in a reduced inversion density and time-averaged output power of the laser. This feature could be observed as an increase of the background non-lasing radiation in the optical spectrum for low repetition frequencies, as seen from Fig. 5. The typical average output power was of the order of 1 mW.

The oscilloscope trace reveals the Gaussian shape of the pulse with a width of ~80 ns nearly independent on the repetition rate. The pulse-to-pulse timing jitter of the Q-switched fiber laser was measured directly from oscilloscope traces. It can be seen from Fig. 6(a) that without modulation-induced stabilization, the Q-switched pulse builds up with a large timing jitter of ~50 μs. By contrast, with the control signal activated, timing jitter remained below 30 ns, as shown in Fig. 6(b). In Fig. 6(a) the oscilloscope has been triggered on one pulse, and the subsequent pulse has been recorded to a histogram for 2 s. In Fig. 6(b) the oscilloscope has been triggered to the control pulse, and the timing jitter of the first pulse was recorded with similar histogram. The technique used in Fig. 6(a) was not possible in this case, since the jitter was too low to be observed at that scale.

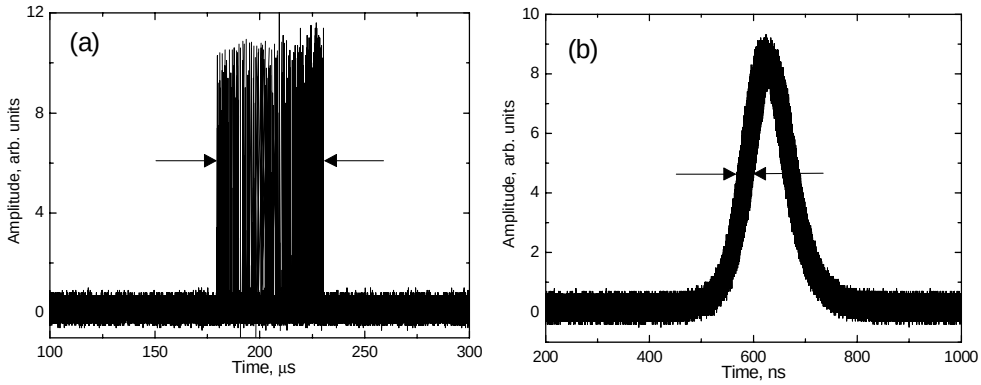

Fig. 6. Timing jitter shown as a histogram recorded for 2 s. With the activated control signal, the timing of the Q-switched pulse is temporally locked to the control pulse resulted in the jitter reduction from 50 μs (a) to 30 ns (b) at the repetition rate of $f_{REPRATE}$=5 kHz. The timing jitter has been defined as shown in the Figure by arrow gap.

#94703 - $15.00 USD Received 4 Apr 2008; revised 22 May 2008; accepted 26 May 2008; published 29 May 2008

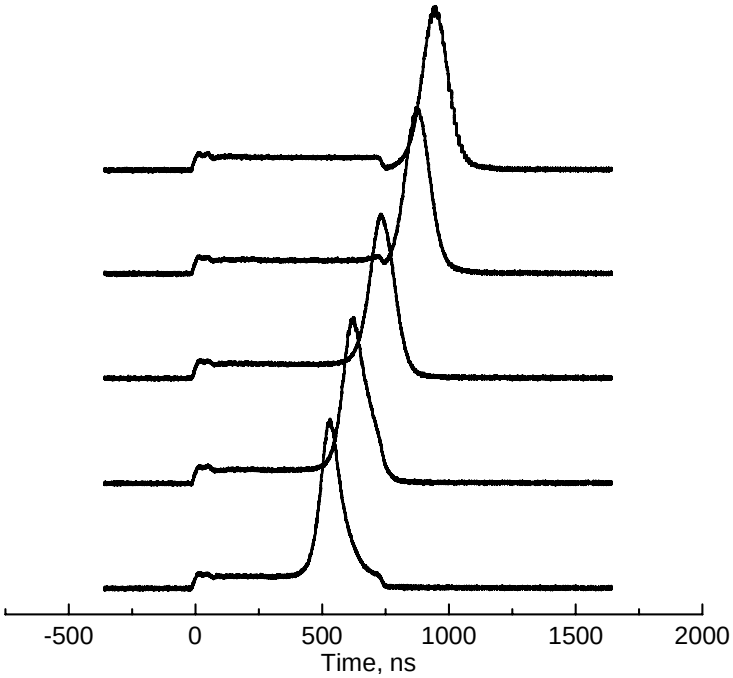

Fig. 7. The relative time location of the control and Q-switched pulses for the locking state. For larger time delay between the pulses, the synchronization of the Q-switched pulse repetition rate to the control signal could not be achieved. (Control and Q-switched pulse amplitudes are not in scale).

Locking performance and timing jitter were further studied by tuning the Q-switched pulse location in the time domain in respect to control pulse for various pump powers. Figure 7 illustrates the range of relative pulse detunings that ensures the pulse synchronization to the locking signal. The control pulse with duration of 750 ns is seen in the figure as a small-amplitude square-shaped pulse superimposed with Gaussian-like Q-switched pulse. The amplitude of the Q-switched pulse in these measurements was strongly attenuated for clarity of the scope traces. The uppermost pulse trace in this figure indicates the largest detuning that still provides the firm pulse locking. For larger shifts, the laser operates in the free-running passive Q-switching mode.

The timing jitter of the locked pulses gradually decreases with the pump power, as seen from Fig. 8. This observation is in agreement with results presented in Fig. 4, where the locking bandwidth $\Delta\Omega_{lock}$ for pulse repetition rate at the fundamental harmonic of modulation frequency ($f_{REPRATE}=f_{MOD}$) is shown to increase with free-running frequency that is proportional to the pump power. Finally, the measurements confirm that the locking bandwidth scales up with the duration of the control pulse, as seen from Fig. 9.

#94703 - $15.00 USD Received 4 Apr 2008; revised 22 May 2008; accepted 26 May 2008; published 29 May 2008

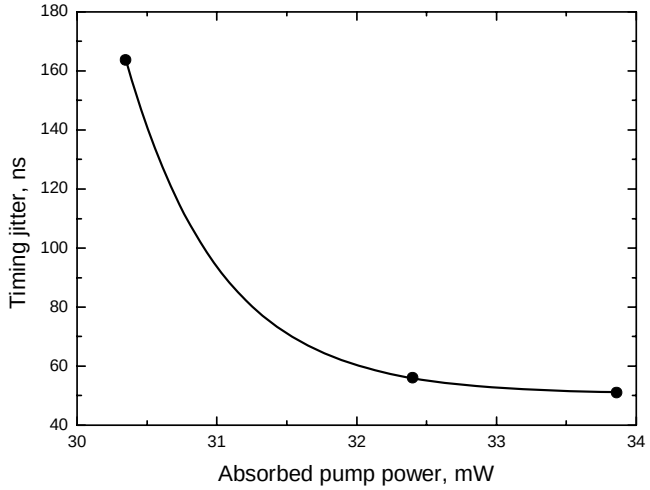

Fig. 8. Timing jitter of the Q-switched pulse train for the locking state versus pump power.

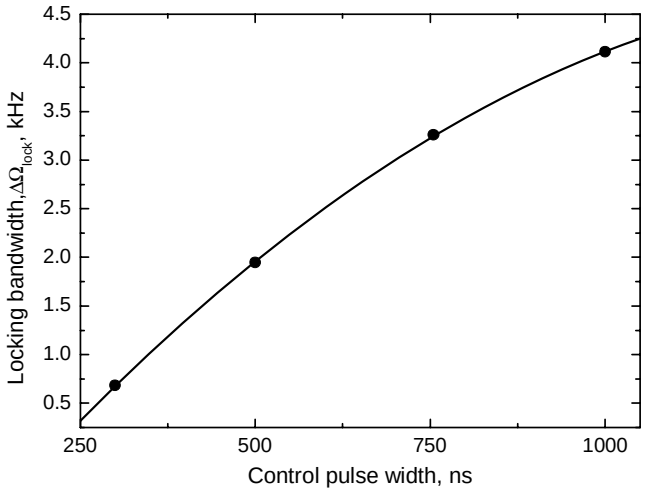

Fig. 9. The dependence of the locking bandwidth $\Delta\Omega_{lock}$ on the control pulse duration.

4. Conclusions

In conclusion, we described a novel technique for controlling Q-switched pulse timing demonstrated experimentally using surface-normal semiconductor modulator in an Yb-doped fiber laser. The dependence of locking bandwidth and pulse timing jitter on the parameters of control pulse and pump power was thoroughly studied. The Q-switched ytterbium fiber laser shows more than by factor of 1.66×10^3 reduction in timing jitter from 50 μs down to 30 ns with the proposed modulation technique.

Acknowledgments

This work was supported by Emil Aaltonen Foundation, Vilho, Yrjö ja Kalle Väisälä Foundation, Finnish Foundation for Technology Promotion, Jenny and Antti Wihuri Foundation, and National Graduate School in Materials Physics. The authors also wish to thank Mr. Tero Kontkanen for designing the control electronics used for modulation.

#94703 - $15.00 USD Received 4 Apr 2008; revised 22 May 2008; accepted 26 May 2008; published 29 May 2008